ROYAL SOCIETY OF CHEMISTRY

PAPER

Check for updates

Exploring N-heterocyclic linked novel hybrid chalcone derivatives: synthesis, characterization, evaluation of antidepressant activity, toxicity assessment, molecular docking, DFT and ADME study†

Hemant S. Deshmukh,*[a] Vishnu A. Adole, [iD] *[a] Sanjay B. Wagh,[b] Vijay M. Khedkar[c] and Bapu S. Jagdale*[a]

In the search for novel antidepressant agents, twelve novel nitrogen-containing heterocycle-linked chalcone derivatives have been synthesized and comprehensively characterized using FT-IR, ^{1}H NMR, ^{13}C NMR, and Mass spectral methods. The synthetic strategy involves the preparation and optimization of reaction conditions for obtaining 4-carbazole-, indole-, and pyrrole-linked acetophenones, which were subsequently coupled with pyrazole aldehydes bearing piperidine, morpholine, benzotriazole, and imidazole ring systems. *In vivo* antidepressant activity of the compounds was evaluated using the Tail Suspension Test (TST) and Forced Swim Test (FST). Chalcone derivatives with a benzo[*d*][1,2,3]triazol-1-yl substituent exhibited significant reductions in immobility times, indicating enhanced antidepressant activity. Chalcone derivatives with piperidin-1-yl and morpholino groups demonstrated relatively lower activity. Molecular docking studies against the human serotonin transporter (hSERT) (PDB code: 5I6X) revealed that the chalcone derivatives exhibited excellent binding affinity (average docking score: −8.540, binding energy: −60.044 kcal mol^{-1}) through favorable van der Waals, electrostatic, and hydrogen bonding interactions (only for **13b**) within the active site. The binding interaction of compound **13b** was particularly strong, with a Glide docking score of −9.120 and binding energy of −65.454 kcal mol^{-1}, highlighting the contribution of both $\pi-\pi$ stacking and hydrogen bonding interactions. Chalcone derivatives showed low acute oral toxicity (LD$_{50}$ > 2000 mg kg^{-1}, category 5) in female Swiss albino mice per OECD 423 guidelines, with no mortality or adverse effects at 300 and 2000 mg kg^{-1}, and normal body weight gain over 14 days. These findings underscore the potential of benzo[*d*][1,2,3]triazol-1-yl-based chalcone derivatives as promising antidepressant agents with a favorable safety profile. Density Functional Theory (DFT) analysis was performed on the most active compound, **13c**, to gain insights into its structural and electronic properties. Additionally, ADME (Absorption, Distribution, Metabolism, and Excretion) profiling of the synthesized compounds indicated favorable drug-like characteristics and balanced pharmacokinetic profiles, supporting their potential as promising candidates for further pharmaceutical development.

[a]*Research Centre in Chemistry, Mahatma Gandhi Vidyamandir's Loknete Vyankatrao Hiray Arts, Science and Commerce College (Affiliated to Savitribai Phule Pune University, Pune), Panchavati, Nashik, Maharashtra, 422003, India. E-mail: hemd144@gmail.com; vishnuadole86@gmail.com; dr.jagdalebs@gmail.com*

[b]*TS Chemistry Solutions, Technology Development of API and API Intermediates, Dyes and Dyes Intermediates & Specialty Chemicals, Taloja, Raigad, Maharashtra, 422005, India. E-mail: sanjay.wagh@tschemisolutions.com*

[c]*School of Pharmacy, Vishwakarma University, Pune, Maharashtra, 410208, India. E-mail: vijay.khedkar@vupune.ac.in*

† Electronic supplementary information (ESI) available. See DOI: https://doi.org/10.1039/d5ra01929j

1 Introduction

The development of novel antidepressant agents has been an area of intense research due to the significant prevalence and impact of depression on global health. Many people worldwide are suffering from depression, a common and crippling mental health condition that severely impacts quality of life.[1] Despite the widespread use of existing antidepressants, significant limitations, such as undesirable side effects, remain a critical concern.[2] This underscores the urgent need for the development of novel therapeutic agents with improved pharmacological properties. In recent years, the design of hybrid organic compounds, which integrate multiple bioactive pharmacophores, has emerged as a promising strategy in medicinal

chemistry.[3] Among these, N-heterocyclic compounds have garnered considerable attention due to their versatile chemical properties and ability to engage in diverse interactions with biological targets, making them valuable scaffolds in drug discovery. The incorporation of N-heterocycles into chalcone derivatives, known for their broad spectrum of biological activities, offers a compelling strategy to enhance therapeutic efficacy, optimize pharmacokinetic profiles, explore novel mechanisms of action in depression treatment, and advance drug development.[4,5]

Chalcones, a crucial class of organic compounds characterized by an α,β-unsaturated carbonyl system, have received significant interest due to their notable biological characteristics.[6–9] These compounds serve as important intermediates in the biosynthesis of flavonoids and isoflavonoids[10] and exhibit a wide range of pharmacological properties, including anti-inflammatory,[11] anticancer,[12] antimicrobial,[13] and antioxidant effects.[14] Integrating nitrogen heterocyclic frameworks into the chalcone structure has been connected with improved biological properties characteristics.[15,16] Because of their wide range of pharmacological characteristics, nitrogen heterocycles are essential for the design and development of pharmaceuticals.[17,18] When paired to the chalcone scaffold, these heterocycles can greatly enhance the pharmacokinetic and pharmacodynamic characteristics of therapeutics.[19] The chalcone structure has been substantially tweaked to include a number of heterocycles that contain nitrogen, including

pyridine, pyrimidine, pyrazole, and indole, leading to better biological activity.[20,21] In past few years, compounds containing carbazole, indole and pyrrole have been investigated for screening antidepressant effects.[22–25] Similarly, hybrid chalcones and those containing heterocyclic moiety like piperidine, morpholine, triazole, etc. have been studied to develop new antidepressant scaffolds.[26–30]

Among the various classes of compounds explored, nitrogen heterocyclic compounds have shown promising antidepressant activities.[31] In addition, such as carbazoles, indoles, pyrroles, piperidines, morpholines, and benzotriazoles have been promising compounds in search of potent antidepressant agents.[32–38] Fig. 1 emphasizes the significance of key nitrogen-containing heterocycles, such as pyrazole, carbazole, indole, pyrrole, piperidine, morpholine, and benzotriazole. These structures are vital in drug discovery and medicinal chemistry because of their diverse and extensive biological activities.

Carbazoles, tricyclic aromatic compounds with a nitrogen atom, exhibit a broad spectrum of biological activities, including anticancer, antimicrobial, and notable antidepressant effects,[39,40] similarly, the indole ring system, a core structure in many natural and synthetic compounds, demonstrates antidepressant activity by interacting with serotonin receptors and modulating the serotoninergic system, crucial for mood regulation.[41] Pyrroles, characterized by a five-membered nitrogen-containing ring, have also shown potential antidepressant effects,[42] while piperidines, six-membered nitrogen-
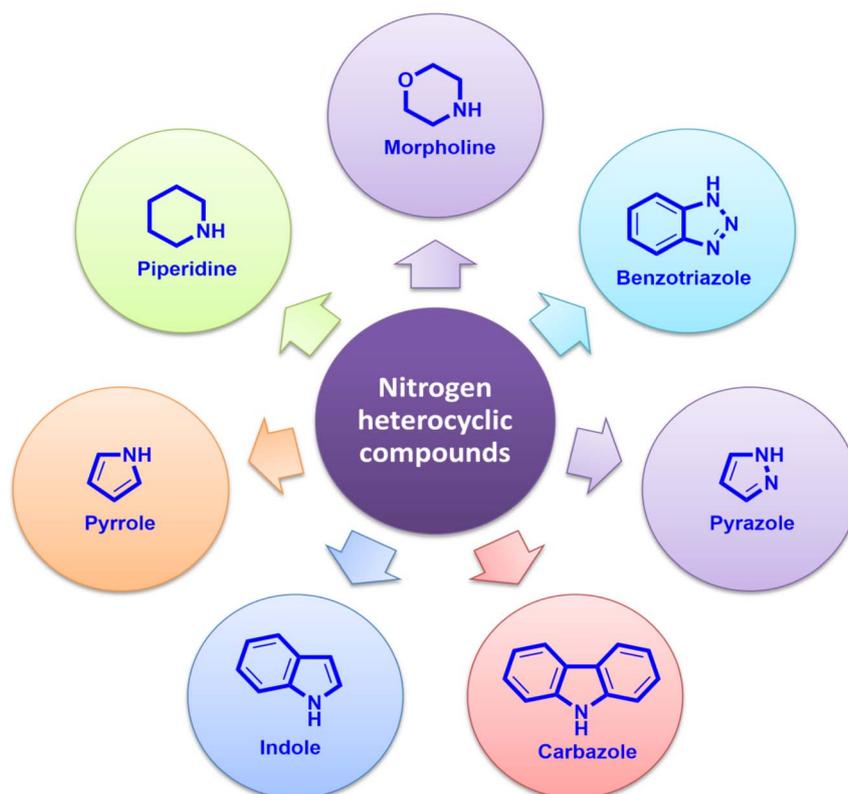

Fig. 1 Key nitrogen heterocycles, including pyrazole, carbazole, indole, pyrrole, piperidine, morpholine, and benzotriazole which play crucial roles in drug discovery and medicinal chemistry due to their wide range of biological activities.
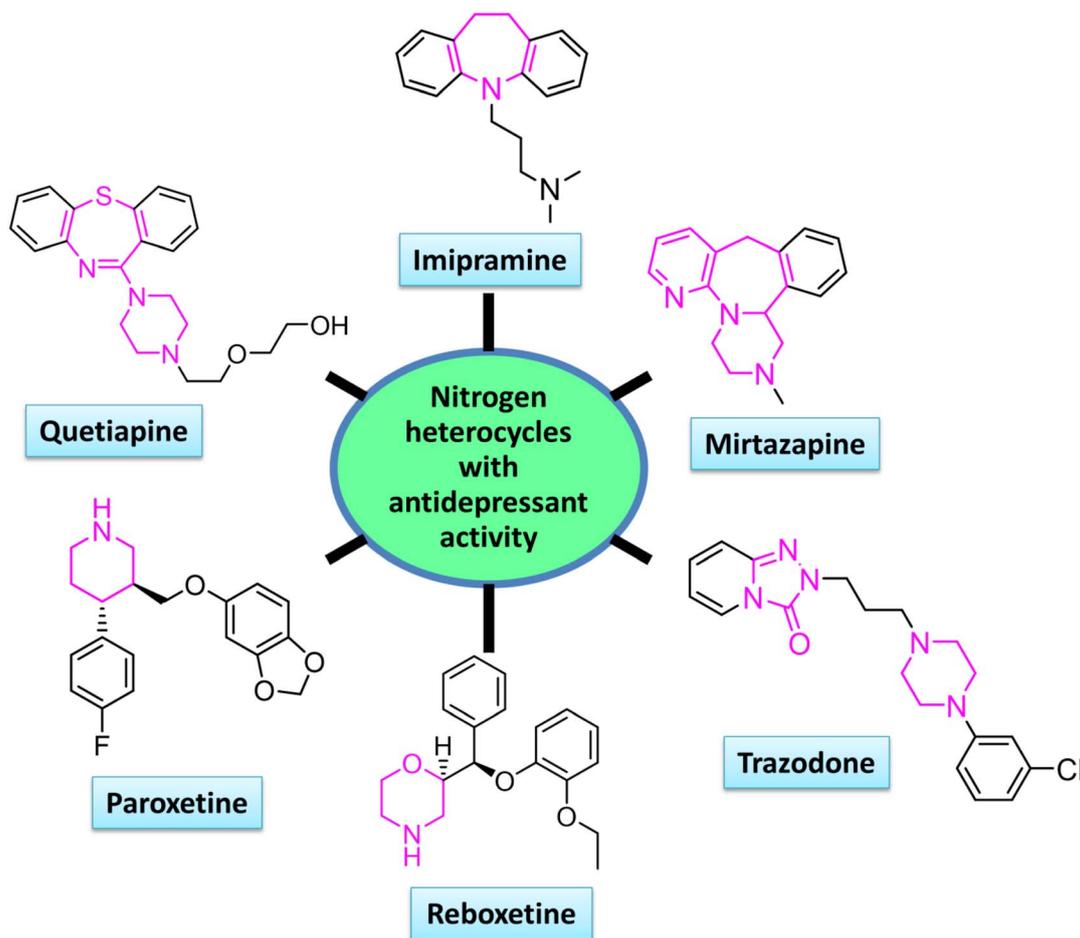
Fig. 2 Chemical structures of selected antidepressant drug molecules containing nitrogen heterocyclic ring structures.

containing heterocycles, and morpholine-containing compounds, featuring both oxygen and nitrogen in a six-membered ring, are recognized for their antidepressant properties.[43,44] Additionally, benzotriazoles, comprising a triazole ring fused with a benzene ring, have emerged as promising antidepressants due to their interactions with neurotransmitter receptors and enzymes implicated in depression.[45] Fig. 2 displays the chemical structures of several commonly prescribed antidepressant drugs, such as tricyclic antidepressants (*e.g.*, imipramine), tetracyclic antidepressants (*e.g.*, mirtazapine), serotonin antagonist and reuptake inhibitors (*e.g.*, trazodone), norepinephrine reuptake inhibitors (*e.g.*, reboxetine), selective serotonin reuptake inhibitors (*e.g.*, paroxetine), and atypical antipsychotics that also exhibit antidepressant effects (*e.g.*, quetiapine). These medications operate through diverse mechanisms, underscoring the structural variety and pharmacological intricacy inherent in antidepressant treatments.[46–52] Compounds **A–F** highlighted in Fig. 3, including 1-(9*H*-carbazol-9-yl)-6-(4-(2-methoxyphenyl)piperazin-1-yl) hexan-1-one (**A**), 1-(4-benzhydrylpiperazin-1-yl)-2-(1*H*-indol-3-yl) ethan-1-one (**B**), 5-(4-bromophenyl)-1-(4-chlorophenyl)-*N*-hydroxy-1*H*-pyrazole-3-carboxamide (**C**), 5-phenyl-*N*-(2-(4-(3-chloro-2-methylphenyl)piperazin-1-yl)ethyl)-1,2-dimethyl-1*H*-

pyrrole-3-carboxamide (**D**), (*E*)-3-(2,4-difluorophenyl)-1-(4-morpholinophenyl)prop-2-en-1-one (**E**), and 1-(3-(4-(2-chlorophenyl)piperazin-1-yl)propyl)-1*H*-benzo[*d*][1,2,3]triazole (**F**), have demonstrated significant antidepressant-like activity in preclinical evaluations.[53–58] Notably, these structures contain structural moieties closely related to the chalcone and heterocycle-based compounds synthesized in our study, highlighting their potential as lead candidates for the development of new antidepressant agents.

The serotonin system is the primary focus of current antidepressant medications, which have drawbacks such delayed therapeutic onset and unpleasant side effects.[59] New antidepressant medication development heavily targets the human serotonin transporter (hSERT), which promotes the absorption of serotonin from the synaptic cleft.[60] The research approach used in this research includes the synthesis and structural characterization of the new chalcone derivatives, evaluation of their acute oral toxicity, assessment of their antidepressant activity using behavioural models that have been proven to work, and molecular docking studies to clarify how they interact with hSERT (5i6x). This all-encompassing strategy enables a careful examination of the therapeutic potential and safety of these new compounds, offering an adequate basis for their
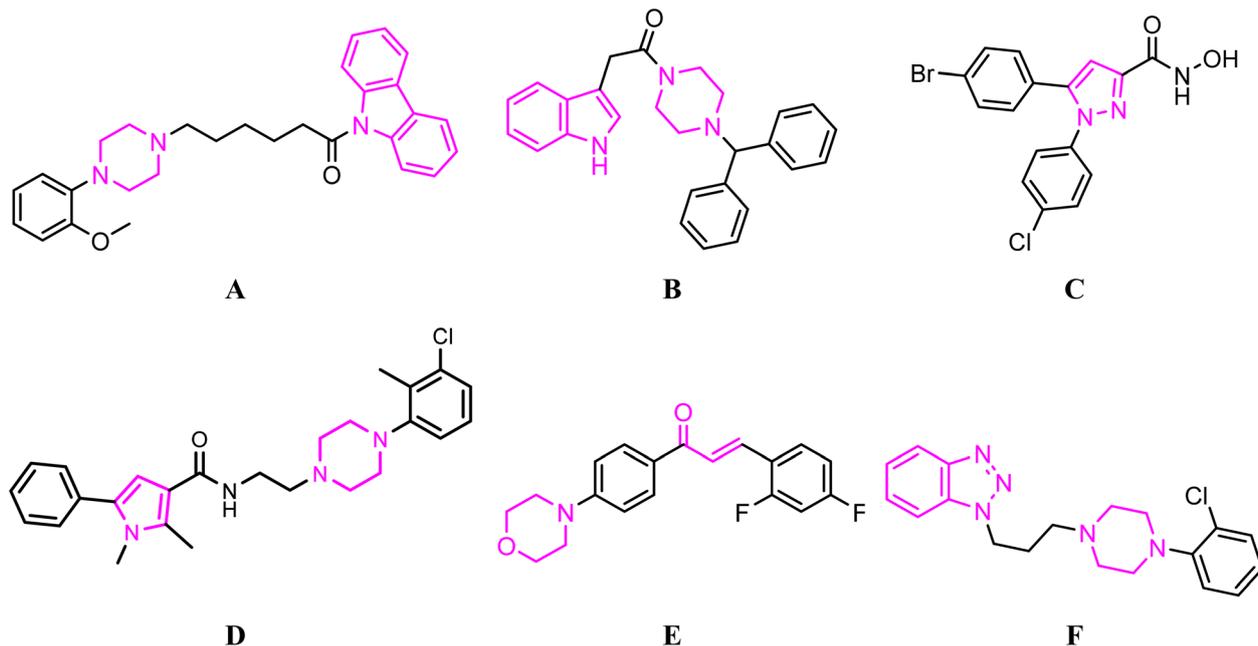
Fig. 3 Structures of compounds A–F, which are structurally related to the synthesized chalcone and heterocycle-based derivatives, showing promising antidepressant-like activity. Pharmacophoric moieties are highlighted in pink.

assessment as possible antidepressants. We report comprehensive results on the synthesis of chalcone derivatives and their evaluation through *in vivo* behavioural assays to assess antidepressant activity. Additionally, acute oral toxicity studies were conducted to determine their safety profile. Molecular docking experiments provided insight into the potential mechanism of action by elucidating the binding interactions between the chalcone derivatives and the human serotonin transporter (hSERT). The findings contribute to the growing body of research on chalcone-based therapeutics and highlight the potential of these compounds as promising candidates for the development of novel antidepressant agents. This study integrates both *in vivo* and *in silico* approaches with the aim of synthesizing and characterizing new nitrogen-containing heterocyclic chalcone derivatives and evaluating their antidepressant potential.

2 Results and discussion

2.1. Chemistry and spectral analysis

Initially, we began our study by exploring the reaction of 9*H*-carbazole (**1**) with 1-(4-fluorophenyl)ethan-1-one (**2**) to synthesize 1-(4-(9*H*-carbazol-9-yl)phenyl)ethan-1-one (**3**). This reaction is significant as it merges the structural motifs of carbazole, known for its diverse biological activities which can enhance the pharmacokinetic properties of the resulting compound. The reaction proceeds through a nucleophilic aromatic substitution mechanism. The nitrogen atom of 9*H*-carbazole attacks the electron-deficient carbon of the aromatic ring in 1-(4-fluorophenyl)ethan-1-one, facilitated by the electron-withdrawing effect of the fluorine substituent leading to the formation of desired compound. Similar reactions of 1*H*-indole

(**4**) and 1*H*-pyrrole (**6**) with compound **2** gave 1-(4-(1*H*-indol-1-yl)phenyl)ethan-1-one (**5**) and 1-(4-(1*H*-pyrrol-1-yl)phenyl)ethan-1-one (**7**). The optimization of reaction conditions for the synthesis of compounds **3**, **5**, and **7** was systematically explored using different solvents, bases, temperatures, and reaction times (Table 1). The results revealed that the choice of base, solvent, and temperature significantly influenced the reaction yield and product formation. For the synthesis of compound **3**, initial attempts using K_2CO_3 and NaH in DMF at 155 °C (entries 1 and 2) resulted in no reaction even after 24–48 hours. Similarly, when the solvent was changed to DMSO and NaH was used at 190 °C (entry 3), a low yield of 20% was obtained, indicating poor reactivity under these conditions. However, a significant improvement was observed when the reaction was carried out in a pressure reactor at 230 °C using NaH as the base in DMF (entry 4), which produced compound **3** in an excellent yield of 92% within 12 hours. This suggests that high temperature and pressure conditions are crucial for achieving high conversion rates in this transformation. For the synthesis of compound **5**, initial trials using K_2CO_3 and NaH in DMF at 155 °C resulted in modest to low yields (entries 5 and 6). The yield increased to 90% when NaH was used as the base at 110–115 °C for 4 hours (entry 7), highlighting the importance of moderate temperature and strong base conditions for successful product formation. The reaction outcome underscores that NaH is more effective than K_2CO_3 under these reaction conditions. In the synthesis of compound **7**, the reaction proved challenging under various conditions. No product formation was observed when K_2CO_3 or NaH was used in DMF or DMSO at reflux temperature for 1 hour (entries 8–11), with tarry mass formation in some cases. Interestingly, a breakthrough was achieved when the reaction was conducted at room temperature with NaH as the base in DMF

**Table 1** Optimization of reaction conditions for the synthesis of compounds **3**, **5** and **7**[a,b]

Entry	Reactants		Solvent	Base[c]	Temperature (°C)	Time (h)	% Yield[d]
1	1	2	DMF	K_2CO_3	155	24	nr
2	1	2	DMF	NaH	155	48	nr
3	1	2	DMSO	NaH	190	48	20
4	1	2	DMF	NaH	230[e]	12	92
5	4	2	DMF	NaH	155	12	25
6	4	2	DMF	K_2CO_3	110–115	4	38
7	4	2	DMF	NaH	110–115	4	90
8	6	2	DMF	K_2CO_3	110–115	1	nr[f]
9	6	2	DMF	NaH	110–115	1	nr[f]
10	6	2	DMSO	NaH	190	1	nr[f]
11	6	2	DMSO	K_2CO_3	110–115	1	nr[f]
12	6	2	DMF	NaH	rt[g]	4	88
13	6	2	DMF	K_2CO_3	rt[g]	4	nr

[a] Where nr – no reaction and rt – room temperature. [b] Reactions on 5 mmol scale of reactants **1**, **2**, **4** and **6**. [c] 5.5 mmol. [d] Isolated yield of pure products. [e] Reaction carried out in a pressure reactor. [f] Reaction produced tarry mass. [g] Reaction started at 0–5 °C for 2 h before stirring at rt.

(entry 12), which afforded an 88% yield after 4 hours. However, the reaction with K_2CO_3 under similar conditions failed to produce any product (entry 13). This indicates that NaH, rather than K_2CO_3, is critical for the success of this transformation and that room temperature conditions are favorable for compound **7** formation. In conclusion, the study highlights the importance of careful selection of reaction parameters, particularly the choice of base and reaction temperature, in optimizing the yield of target compounds. NaH emerged as the superior base over K_2CO_3, and high temperature and pressure were essential for the successful synthesis of compound **3**, while moderate temperatures facilitated the formation of compound **5**, and room temperature was optimal for compound **7**.

The ethyl 3-oxobutanoate (**8**) and phenylhydrazine (**9**) were reacted to produce 5-methyl-2-phenyl-2,4-dihydro-3H-pyrazol-3-one (**10**), an essential step in the synthesis of many pyrazole derivatives. This reaction is conducted in ethanol under reflux conditions, which help ethyl acetoacetate and phenylhydrazine condense. After performing Vilsmeier–Haack formylation with DMF and $POCl_3$, the synthesised pyrazoline **10** yielded 5-chloro-3-methyl-1-phenyl-1H-pyrazole-4-carbaldehyde (**11**). The synthesis of 5-chloro-3-methyl-1-phenyl-1H-pyrazole-4-carbaldehyde derivatives through nucleophilic substitution reactions with various amines under basic conditions represents a versatile approach to functionalizing the pyrazole scaffold. This study explores the reactivity of compound **11** with

piperidine, morpholine, 1H-benzo[d][1,2,3]triazole, and 1H-imidazole, yielding a series of novel pyrazole derivatives with potential applications in medicinal chemistry. The reaction of compound **11** with piperidine under basic conditions resulted in the formation of 3-methyl-1-phenyl-5-(piperidin-1-yl)-1H-pyrazole-4-carbaldehyde (**12a**). This transformation involves the substitution of the chlorine atom by the nucleophilic nitrogen of piperidine. Similarly, the reaction of compound **11** with morpholine under analogous conditions afforded 3-methyl-5-morpholino-1-phenyl-1H-pyrazole-4-carbaldehyde (**12b**). The reaction of compound **11** with 1H-benzo[d][1,2,3]triazole resulted in the formation of 5-(1H-benzo[d][1,2,3]triazol-1-yl)-3-methyl-1-phenyl-1H-pyrazole-4-carbaldehyde (**12c**). Finally, the reaction with 1H-imidazole yielded 5-(1H-imidazol-1-yl)-3-methyl-1-phenyl-1H-pyrazole-4-carbaldehyde (**12d**). The successful synthesis of carbaldehydes (**12a**–**12d**) demonstrates the versatility of compound **11** as a synthetic precursor. The reactions of compounds **3**, **5**, and **7** with carbaldehydes **12a**–**12d** were carried out under basic conditions in methanol to synthesize the corresponding chalcones (**13a**–**13c**, **14a**–**14c** and **15a**–**15c**). The reactions proceeded smoothly, and the expected chalcones were obtained in good yields. The reactions with carbaldehydes **12a**–**12c** gave the expected chalcones in excellent yields. The structures of the chalcones were confirmed by FT-IR, ^1H NMR, ^{13}C NMR, HRMS methods (only selected compounds) and mass, showing characteristic peaks for the chalcone
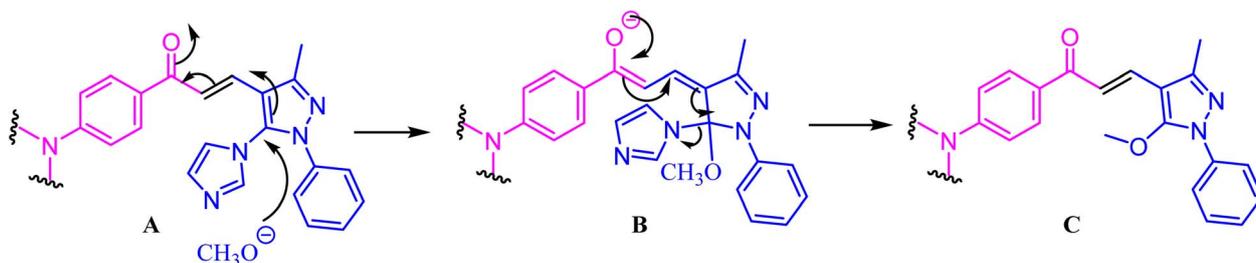
Scheme 1 Probable reaction mechanism for the substitution of imidazole ring by a methoxy group.

framework. In contrast, the reaction with carbaldehyde **12d** did not yield the expected chalcone. Instead, a product was obtained where the imidazole ring was substituted by a methoxy group. This unexpected product was isolated and characterized using IR, ^{1}H NMR, ^{13}C NMR and mass spectral methods, revealing the methoxy substitution. The Scheme 1 depicts the plausible reaction pathway for the substitution of imidazole ring by a methoxy group. The reaction begins with the methoxy group attacking the chalcone framework **A** at the carbon bearing imidazole ring, forming a tetrahedral intermediate **B**. This intermediate then loses the imidazole ring, resulting in the formation of the corresponding chalcone structure **C**. The reaction with carbaldehyde **12d**, however, revealed an intriguing deviation, highlighting the reactivity of the imidazole ring under the given conditions. The unexpected substitution of the imidazole ring with a methoxy group can be rationalized by a proposed reaction mechanism, suggesting a possible side reaction pathway in the presence of methanol and base. This observation highlights the critical role of solvent effects and nucleophile availability in synthetic design, as they can lead to unanticipated product outcomes.

The synthetic intermediates 1-(4-(9H-carbazol-9-yl)phenyl) ethan-1-one (**3**), 1-(4-(1H-indol-1-yl)phenyl)ethan-1-one (**5**), 1-(4-(1H-pyrrol-1-yl)phenyl)ethan-1-one (**7**), and pyrazole cabaldehydes (**12a–12d**) were characterized by ^{1}H NMR and ^{13}C NMR methods. The ^{1}H NMR spectrum of compound **3** displayed signals characteristic of aromatic protons and a methyl group. The aromatic proton signals appeared as multiplets between 8.21 and 7.30 δ. The ^{13}C NMR spectrum revealed the presence of aromatic carbon signals in the range of 142.20–109.79 δ. The methyl group was observed at 2.70 δ in ^{1}H NMR and 26.72 δ in ^{13}C NMR spectrum. A signal at 197.00 δ was attributed to a ketone carbonyl carbon. The compound **5** showed aromatic signals between 8.21 and 7.30 δ in ^{1}H NMR and 142.20 to 109.79 δ in ^{13}C NMR spectrum. The ketone carbonyl was located at 196.83 δ and methyl group at 26.59 δ. The compound **7** was found to show aromatic proton signals between 8.03 and 6.35 δ and aromatic carbon signals between 144.05 and 111.64 δ. The signal at 196.77 δ is attributed to the ketone carbonyl carbon. The ^{1}H NMR spectrum of pyrazole carbaldehydes (**12a–12d**) showed aldehyde proton signal between 9.78 and 10.01 δ as a sharp singlet. This carbonyl group
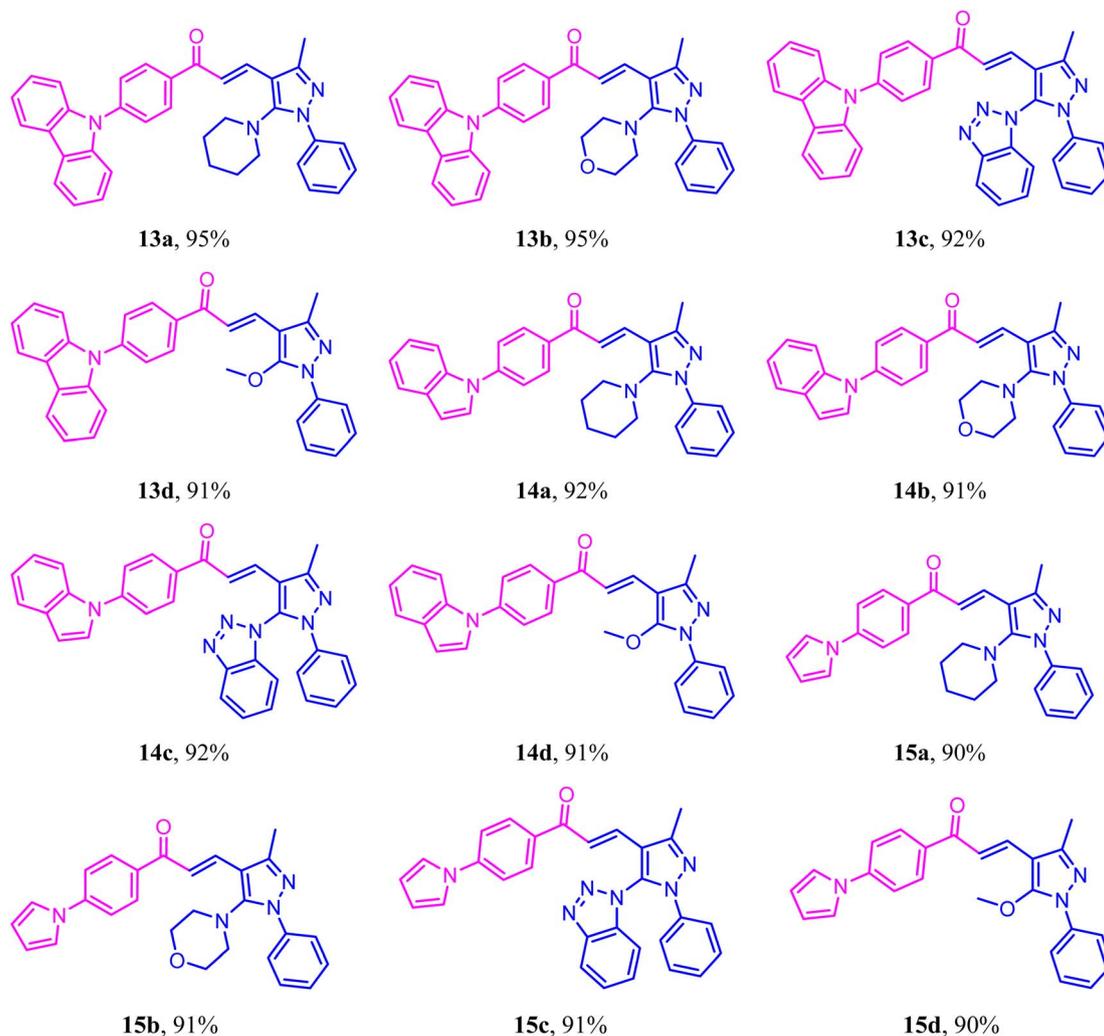

Fig. 4 Structural diversity of the synthesized compounds.

was observed at 183.67–183.20 δ in its ^{13}C NMR spectrum. The phenyl ring attached to the pyrazole moiety exhibited multiplets in the aromatic region of the ^1H NMR spectrum, confirming its aromatic nature. This was further corroborated by the presence of aromatic carbons in the phenyl ring observed in the ^{13}C NMR spectrum. Compound **12a** features a piperidinyl ring, evidenced by signals at 1.55 δ for six protons and 3.11 δ for four protons in the ^1H NMR spectrum. The carbon signals corresponding to the piperidinyl ring ranged between δ 52.40 and 14.12 in the ^{13}C NMR spectrum. In contrast, compound **12b**, which contains a morpholine ring, exhibited methylene group protons at 3.70–3.68 δ and δ 3.16–3.14 δ. The structures of the other two carbaldehydes, **12c** and **12d**, were also confirmed based on their spectral data. The synthesized chalcones exhibit important stretching frequencies for sp^2 C–H bonds around 3050 cm^{-1}. The sp^3 C–H bonds (CH$_3$ group) in the chalcones showed stretching frequencies between 2820 and 2930 cm^{-1}. The carbonyl (C=O) group in the chalcones is observed with stretching frequencies in the range of 1650–1680 cm^{-1}. The chalcones displayed C=C stretching frequencies around 1620–1630 cm^{-1}. Additional significant stretching frequencies for the chalcones' C=C bonds are found between 1500 and 1600 cm^{-1}. In all synthesized chalcones, the *trans* stereochemistry was confirmed by the observation of a coupling constant, $J = 15.6$ Hz. For all synthesised chalcones, the coupling constant values near $J = 8$–9 Hz for two mutually linked ortho protons of the benzene ring clearly show the para disubstitution pattern. It has been found that the ketone carbonyl, which is conjugated with an unsaturated system, exhibits a ^{13}C NMR signal at approximately 190 δ. The aromatic section of the corresponding NMR spectra contained the signals for aromatic carbon atoms and aromatic protons. The methyl group in every synthesised chalcone was identified in the carbon NMR spectrum approximately at 14 δ and in the proton NMR spectrum nearly at 2.70 δ. Mass spectrometry confirmed the exact molecular weights and molecular formula of the synthesized chalcones. The structural diversity of the synthesized compounds is given in Fig. 4.

2.2. Acute oral toxicity study

The acute oral toxicity of the synthesized compounds (**13a–13c**) was evaluated in accordance with the OECD 423 guidelines, employing a scientifically rigorous and systematic approach to assess their toxicity profile (Table 2). The study utilized female Swiss albino mice as the experimental model, chosen for their well-documented sensitivity and relevance in toxicological research. A stepwise dosing protocol was implemented, commencing with an initial dose of 300 mg kg^{-1} body weight and escalating to a higher dose of 2000 mg kg^{-1}, administered *via* oral gavage to ensure precise and controlled delivery. In the first phase of the study, three groups of three mice each were administered the synthesized compounds at the 300 mg kg^{-1} dose level. Post-administration, the animals were meticulously monitored for immediate and delayed toxicological responses. Observations were conducted immediately after dosing, followed by assessments at 30-minute intervals, and periodically over the first 24 hours. This intensive monitoring regimen was sustained daily for a total of 14 days, during which the mice were evaluated for any signs of toxicity, behavioral alterations, and mortality. Notably, no mortality or signs of intoxication were observed at the 300 mg kg^{-1} dose level, and all animals exhibited normal behavioral and physiological parameters throughout the observation period. In the subsequent phase, the dose was escalated to 2000 mg kg^{-1}, and the experimental protocol was repeated with three new groups of three mice each. Consistent with the findings from the initial phase, no mortality or adverse clinical signs were observed at this higher dose level. The absence of acute toxic effects at both 300 mg kg^{-1} and 2000 mg kg^{-1} dose levels suggests that the synthesized compounds exhibit a favorable safety profile within the tested range. These findings underscore the potential low toxicity of the synthesized compounds and provide a robust foundation for further preclinical evaluation. The study's adherence to internationally recognized guidelines, combined with its systematic and detailed observational approach, enhances the reliability and scientific rigor of the results, making a compelling case for the continued investigation of these compounds in subsequent stages of drug development.

Body weight measurements were systematically recorded to evaluate the potential impact of the synthesized compounds on the growth and overall health of the experimental animals. Pre-administration fasting weights were obtained prior to dosing, followed by measurements on days 7 and 14 post-treatment to monitor any deviations from normal growth patterns. The data revealed a consistent and progressive weight gain across all treatment groups, reinforcing the absence of adverse effects associated with the synthesized compounds. Specifically, in the group administered 300 mg kg^{-1}, the initial body weights on day 0 ranged from 21.5 g to 25 g. By day 7, the weights increased to a range of 26.5 g to 29.5 g, and by day 14, the weights further

Table 2 Experimental design for acute oral toxicity study of synthesized compounds (**13a–13c**) in Swiss albino mice, including test doses, concentrations, and dosage volumes administered in stepwise protocol

Step	Compounds	Animal ID	Test dose (mg kg^{-1})	Test concentration (mg mL^{-1})	Dosage mice (ml kg^{-1})
I	**13a**	1, 2, 3	300	200	10
	13b	4, 5, 6	300	200	10
	13c	7, 8, 9	300	200	10
II	**13a**	1, 2, 3	2000	200	10
	13b	4, 5, 6	2000	200	10
	13c	7, 8, 9	2000	200	10

rose to 30 g to 36 g. Similarly, in the group treated with the higher dose of 2000 mg kg^{-1}, the initial body weights on day 0 ranged from 21.5 g to 24.5 g, increasing to 27 g to 30.5 g by day 7, and reaching 32 g to 35 g by day 14. This steady and consistent weight gain across both dose levels aligns with normal growth trajectories, indicating that the synthesized compounds did not interfere with the animals' metabolic or physiological processes. In addition to body weight measurements, clinical observations were meticulously conducted and documented throughout the study period. No signs of toxicity, distress, or abnormal behavior were observed in any of the animals. All mice remained active, displayed normal grooming habits, and exhibited no clinical symptoms indicative of adverse effects. The absence of such signs, coupled with the consistent weight gain, provides compelling evidence of the safety and biocompatibility of the synthesized compounds at the tested doses. These findings not only highlight the non-toxic nature of the compounds but also underscore their potential for further development. The systematic and detailed approach to monitoring body weight and clinical signs enhances the scientific rigor of the study, offering robust support for the safety profile of the synthesized compounds in preclinical settings.

In accordance with the Globally Harmonized System (GHS) for the classification of chemicals based on acute toxicity, the synthesized compounds (**13a–13c**) were classified under category 5, which is defined by an LD$_{50}$ range of 2000–5000 mg kg^{-1}. This classification represents the least hazardous category, signifying low acute oral toxicity. The categorization was determined based on the absence of mortality and the lack of any significant adverse clinical signs at the highest tested dose of 2000 mg kg^{-1} (Table 3). These results demonstrate that the synthesized compounds exhibit a high safety margin in acute oral exposure scenarios, as no toxic effects were observed even at substantial doses. The study's findings are further supported by the consistent body weight gain and normal clinical observations across all treatment groups, reinforcing the compounds' benign nature (Table 4). The absence of toxicity at doses up to 2000 mg kg^{-1} suggests that the LD$_{50}$ value exceeds this threshold, placing the compounds in a low-risk category for acute oral toxicity. This conclusion is aligned with the study's rigorous adherence to internationally recognized guidelines, such as the OECD 423 protocols, ensuring the reliability and scientific validity of the data. The absence of adverse effects at high doses, coupled with the systematic and detailed experimental approach, underscores the compounds' suitability for further development and regulatory approval. In summary, the synthesized compounds demonstrate a favorable safety profile for acute oral exposure, with no observed toxicity at doses up to

2000 mg kg^{-1}. These findings are crucial for regulatory submissions, safety evaluations, and the development of guidelines aimed at ensuring compliance with human and environmental health standards.

2.3. *In vivo* antidepressant activity

The evaluation of the antidepressant activity of novel chalcone derivatives reveals significant insights into the influence of different substituents on the pharmacological efficacy of these compounds. The compounds were assessed using the Tail Suspension Test (TST) and Forced Swim Test (FST), with the duration of immobility serving as a measure of antidepressant activity; lower immobility times indicate higher activity. The study includes twelve chalcone derivatives (compounds **13a–13d**, **14a–14d**, **15a–15d**), a disease control group, and a positive control group treated with fluoxetine. Table 5 summarizes the antidepressant activity and molecular docking parameters of the synthesized compounds (**13a–13d**, **14a–14d**, and **15a–15d**). Starting with the carbazole derivatives, compound **13a**, which includes a piperidin-1-yl group, showed immobility times of 409.83 seconds in the TST and 220.83 seconds in the FST. These high immobility times suggest that this compound has relatively low antidepressant activity. In comparison, compound **13b**, which contains a morpholino group, demonstrated slightly lower immobility times of 385.66 seconds in the TST and 225.5 seconds in the FST, indicating a minor increase in

Table 4 Body weight analysis

Step & dose	Compounds	Animal ID	Day 0	Day 7	Day 14
Step I 300 mg kg^{-1}	**13a**	1	22.5	28	32
		2	21.5	26.5	33
		3	25	29	34.5
	13b	4	21	26.5	32.5
		5	23.5	29	36
		6	24	29.5	34.5
	13c	7	21.5	26.5	30
		8	22.5	26.5	31
		9	23.5	26.5	31
Step II 2000 mg kg^{-1}	**13a**	1	24	29.5	33
		2	23.5	29	32.5
		3	24	30	35
	13b	4	23	27.5	32
		5	24.5	30.5	34.5
		6	21.5	27	32
	13c	7	22	28	33.5
		8	22	28.5	33.5
		9	23.5	29.5	34.5

Table 3 Summary of acute oral toxicity study results for synthesized compounds

Step	Dose (mg kg^{-1})	No. of treated mice	Terminally sacrificed	Found dead (X)
1	**300**	9	9	0
2	**2000**	9	9	0
TOTAL	—	18	18	0

Table 5 Antidepressant activity of the synthesized compounds (**13a**–**13d**, **14a**–**14d** and **15a**–**15d**)

Code	Duration of immobility[a] (s) (mean ± SEM)[b]		DID (%)	
	Tail suspension test	Forced swim test	Tail suspension test	Forced swim test
13a	409.83 ± 45.635	220.83 ± 16.37	5.74	24.92
13b	385.66 ± 11.92	225.5 ± 21.23	11.30	23.47
13c	284.33 ± 27.45	188.66 ± 16.29	34.67	35.63
13d	397.66 ± 14.25	234.33 ± 18.69	8.55	13.59
14a	423.66 ± 52.28	244.16 ± 44.89	2.58	16.61
14b	426.5 ± 31.59	286.5 ± 49.70	1.92	2.22
14c	393 ± 28.61	240.83 ± 12.11	9.60	17.90
14d	410.66 ± 34.99	253.16 ± 22.71	5.57	13.62
15a	415.16 ± 18.55	273.83 ± 49.07	4.50	6.55
15b	409.83 ± 45.63	259.16 ± 33.99	5.74	11.56
15c	371 ± 20.99	225.66 ± 26.07	14.60	22.99
15d	364.33 ± 29.81	227 ± 22.67	16.24	22.53
Disease control	434.83 ± 26.97	293 ± 39.06	—	—
Fluoxetine	175 ± 27.05	128.33 ± 23.09	59.67	56.17

[a] Duration of immobility measured in seconds during the tail suspension test and forced swim test. [b] Values are represented as the mean ± standard error of the mean (SEM) from independent experiments.

antidepressant activity compared to **13a**. Notably, compound **13c**, which features a benzo[*d*][1,2,3]triazol-1-yl group, exhibited significantly lower immobility times of 284.33 seconds in the TST and 188.66 seconds in the FST, indicating a marked enhancement in antidepressant activity. This suggests that the benzo[*d*][1,2,3]triazol-1-yl group plays a critical role in enhancing the efficacy of the compound. Compound **13d**, which includes a methoxy group, showed intermediate activity with immobility times of 397.66 seconds in the TST and 234.33 seconds in the FST, indicating it is less effective than **13c** but better than **13a** and **13b**. For the indole derivatives, compound **14a**, which has a piperidin-1-yl group, demonstrated immobility times of 423.66 seconds in the TST and 244.16 seconds in the FST. These results are similar to those of compound **13a**, indicating low antidepressant activity. Compound **14b**, featuring a morpholino group, showed even higher immobility times of 426.5 seconds in the TST and 286.5 seconds in the FST, suggesting even lower activity compared to **14a**. However, compound **14c**, which includes a benzo[*d*][1,2,3]triazol-1-yl group, demonstrated improved activity with immobility times of 393 seconds in the TST and 240.83 seconds in the FST, highlighting the beneficial impact of this substituent on the compound's antidepressant activity. Compound **14d**, which contains a methoxy group, showed immobility times of 410.66 seconds in the TST and 253.16 seconds in the FST, indicating slightly better activity than compounds **14a** and **14b**, yet less effective than **14c**. Among the pyrrole derivatives, compound **15a**, which includes a piperidin-1-yl group, showed immobility times of 415.16 seconds in the TST and 273.83 seconds in the FST. These times suggest that this compound has relatively low antidepressant activity. Compound **15b**, which features a morpholino group, demonstrated similar immobility times of 409.83 seconds in the TST and 259.16 seconds in the FST, indicating comparable activity to **15a**. Notably, compound **15c**, which includes a 1*H*-inden-1-yl group, exhibited improved

activity with immobility times of 371 seconds in the TST and 225.66 seconds in the FST, highlighting the positive impact of this substituent. Compound **15d**, featuring a methoxy group, showed further improved activity with immobility times of 364.33 seconds in the TST and 227 seconds in the FST, indicating it is more effective than compounds **15a** and **15b** but slightly less effective than **15c**.

The data clearly demonstrate that the nature and position of substituents significantly affect the antidepressant activity of chalcone derivatives. The benzo[*d*][1,2,3]triazol-1-yl group, present in compounds **13c** and **14c**, consistently showed better activity across different core structures (carbazole and indole), suggesting that this group enhances interaction with the biological target, possibly by improving binding affinity or optimizing pharmacokinetic properties. The methoxy group also showed moderate improvement in activity but was less effective than the benzo[*d*][1,2,3]triazol-1-yl group. On the other hand, the piperidin-1-yl and morpholino groups generally resulted in higher immobility times, indicating lower antidepressant activity. These results suggest that these substituents may not be favorable for enhancing antidepressant properties in the chalcone derivatives tested. The disease control group, which did not receive any active treatment, showed the highest immobility times (434.83 seconds in the TST and 293 seconds in the FST), serving as a baseline for comparison. The positive control group treated with fluoxetine, a well-known antidepressant, showed significantly lower immobility times (175 seconds in the TST and 128.33 seconds in the FST), validating the effectiveness of the behavioral assays used in this study. In conclusion, the study highlights the critical role of substituent modifications in influencing the antidepressant activity of chalcone derivatives. The % DID (Percentage Decrease in Duration) values reveal the effectiveness of different compounds in reducing immobility in the tail suspension and forced swim tests compared to the disease control. In the tail

suspension test, most compounds exhibit moderate to high reductions in immobility, with DID values ranging from 1.92% to 34.67%, indicating varying degrees of antidepressant-like activity. Compounds **13c** and **15d** show particularly notable reductions, suggesting strong potential for antidepressant effects. In the forced swim test, the DID values are generally lower, ranging from 2.22% to 56.17%, with fluoxetine demonstrating the highest decrease in immobility, reflecting its well-established antidepressant efficacy. The benzo[*d*][1,2,3]triazol-1-yl group emerged as a particularly effective substituent for enhancing antidepressant activity, suggesting its potential as a key pharmacophore for the development of more potent chalcone-based antidepressants. Conversely, substituents such as the piperidin-1-yl and morpholino groups were associated with lower activity, indicating the need for careful selection and optimization of substituents in the design of novel chalcone derivatives for antidepressant therapy. Future research should focus on further structural modifications and detailed mechanistic studies to elucidate the precise interactions between these compounds and their biological targets, ultimately guiding the development of more effective and selective antidepressant agents.

2.4. Molecular docking investigation

Molecular docking is now considered to be an integral component of drug discovery to elucidate the binding mechanism, especially in the lack of resources to perform the target based assays, imparting knowledge on binding affinities, mode of orientation and the associated thermodynamic interactions with the enzyme that could govern the inhibition of the causative pathogen. Thus in order to elucidate the plausible mechanism for antidepressant activity demonstrated by the synthesised chalcones, molecular docking study was performed against of human serotonin transporter receptor (PDB code: 5I6X). The human serotonin transporter (hSERT) is a membrane protein that facilitates the reuptake of serotonin (5-HT) from the synaptic cleft back into the presynaptic neuron, thus terminating serotonin signalling. It is a key target for many antidepressants including selective serotonin reuptake inhibitors (SSRIs). SSRIs block hSERT, increasing serotonin levels in the synapse and alleviating symptoms of depression. The binding affinity data showed that all the chalcone derivatives (**13a–13d**, **14a–14d** and **15a–15d**) were well confined within the active site of hSERT exhibiting excellent binding affinity (average docking score: −8.540 and binding energy −60.044 kcal mol^{-1}) (Table 6) through the formation of bonded and non-bonded interactions. A perusal of the per-residue interaction analysis for one of the most active analogs **13b** (Glide docking score: −9.120, Glide binding energy of −65.454 kcal mol^{-1}) provides insights into the most significant thermodynamic interaction influencing the binding affinity (Fig. 4). The lowest energy conformation of **13b** (Fig. 5) showed that it could snugly fit into the active site of hSERT engaging in energetically favourable interactions. The compound was seen to be buried into the active site engaging in a network of favourable van der Waals interactions with the Phe556(−1.816 kcal mol^{-1}), Gly498(−1.023 kcal mol^{-1}), Glu494(−1.224 kcal mol^{-1}), Glu493(−2.785 kcal mol^{-1}), Ser336(−1.952 kcal mol^{-1}), Phe335(−3.587 kcal mol^{-1}), Phe334(−1.396 kcal mol^{-1}), Gln332(−5.394 kcal mol^{-1}), Ala331(−2.583 kcal mol^{-1}), Asp328(−1.172 kcal mol^{-1}), Arg104(−2.672 kcal mol^{-1}), Asn101(−1.71 kcal mol^{-1}), Gly100(−1.379 kcal mol^{-1}) and Trp103(−1.154 kcal mol^{-1}) through the 1-(4-(9*H*-carbazol-9-yl)phenyl) side chain of prop-2-en-1-one while the 3-(3-methyl-5-morpholino-1-phenyl-1*H*-pyrazol-4-yl) side chain attached to prop-2-en-1-one showed similar interactions with Thr497(−1.319 kcal mol^{-1}), Gly442(−1.013 kcal mol^{-1}), Ser438(−1.934 kcal mol^{-1}), Phe341(−1.387 kcal mol^{-1}), Gly338(−1.349 kcal mol^{-1}), Tyr176(−3.995 kcal mol^{-1}), Tyr175(−1.318 kcal mol^{-1}), Ala173(−1.316 kcal mol^{-1}), Ile172(−3.446 kcal mol^{-1}), Ala169(−1.811 kcal mol^{-1}), Leu99(−1.483 kcal mol^{-1}), Asp98(−1.886 kcal mol^{-1}), Ala96(−1.068 kcal mol^{-1}) and Tyr95(−3.261 kcal mol^{-1}) residues. The enhanced of **13b** is also attributed to favourable electrostatic interactions observed with Thr497(−2.786 kcal mol^{-1}), Glu493(−1.89 kcal mol^{-1}), Phe335(−1.249 kcal mol^{-1}), Gln332(−1.225 kcal mol^{-1}), Tyr176(−1.369 kcal mol^{-1}), Tyr175(−1.245 kcal mol^{-1}), Arg104(−2.764 kcal mol^{-1}) and Asp98(−2.841 kcal mol^{-1}) residues lining the active site. While these favourable van der Waals

Table 6 Molecular docking parameters of the synthesized compounds (**13a–13d**, **14a–14d** and **15a–15d**)

| Code	Glide energy (kcal mol^{-1})	Hydrogen bond (Å)	Pi-stacking (Å) (π–π; cation–π)
13a	−63.273		Phe341(5.269), Phe335(4.060), Arg104(5.372, 4.151,4.265); Arg104(5.573, 5.286)
13b	−65.454	Tyr175 (2.245)	Phe341(5.269), Phe335(4.046), Arg104(5.372, 4.151, 4.265); Arg104(5.573, 5.286)
13c	−66.36		Tyr116(4.888, 5.021), Phe335(4.112), Arg104(5.334, 4.127, 4.281); Arg104(5.584, 5.260)
13d	−61.413	Tyr176(4.967), Phe335(4.989), Arg104(3.590, 3.827)
14a	−59.35		Phe341(5.343), Phe335(4.176), Arg104(5.262, 4.070); Arg104(5.225)
14b	−54.148		Phe341(4.960), Phe335(4.728), Arg104(3.511), Tyr95(5.543)
14c	−60.276		Phe341(5.075), Phe335(4.052), Arg104(4.212), Tyr95(5.420); Arg104(5.299)
14d	−58.477		Phe335(4.240), Arg104(5.318, 4.110), Tyr176(5.208); Arg104(5.266)
15a	−55.875		Phe335(4.202), Arg104(4.582, 4.499)
15b	−56.373		Phe335(5.492), Arg104(3.713), Tyr176(5.051)
15c	−56.578		Phe335(5.375), Arg104(3.973), Tyr95(5.228)
15d	−62.962		Phe335(5.233), Arg104(4.116), Tyr176(5.147)
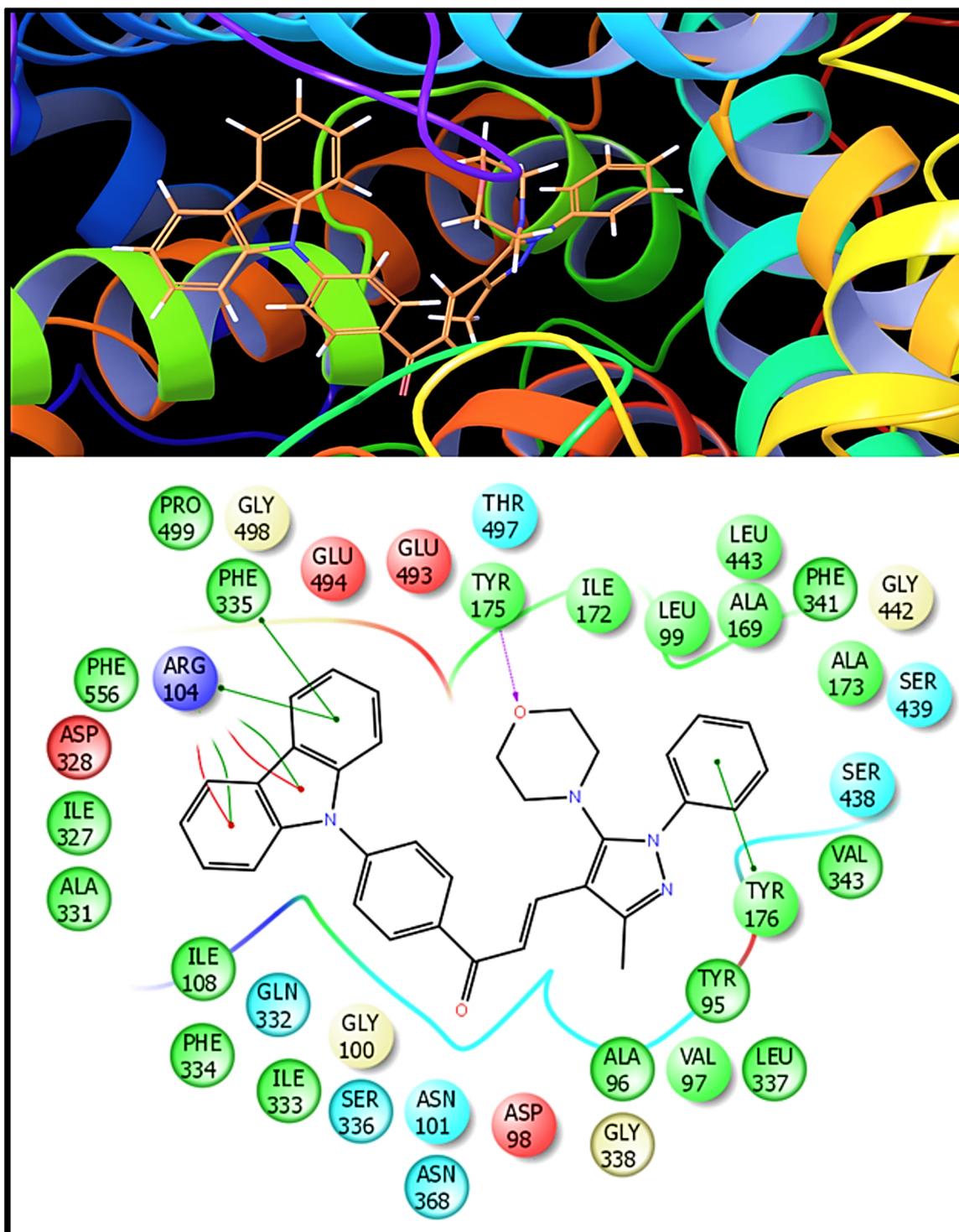
Fig. 5 Binding mode of **13b** into the active site of Human Serotonin Transporter (on bottom side: pink lines represent hydrogen bonding interactions, green lines represent the pi–pi stacking interactions while red lines signify cation–pi stacking interactions).

and electrostatic interactions were seen to be the major driving force in governing the binding, **13b** was also seen to be engaged in very close hydrogen bonding interactions with Tyr175(2.245 Å) through the morpholine (–O–) substituent. Further the compound also exhibited pi–pi stacking interactions with Phe341(5.269 Å), Phe335(4.046 Å), Arg104(5.372 Å, 4.151 Å,

4.265 Å) and cation–pi interactions with Arg104(5.573 Å, 5.286 Å). Such hydrogen bonding and pi-stacking interactions serve as anchors to guide the orientation of the ligand into the 3D space of the active site and facilitate the non-bonded (steric and electrostatic) interactions with active site residues. Similarly, the other chalcone derivatives also exhibited a network of

Fig. 6 Binding mode of **13c** into the active site of Human Serotonin Transporter (on bottom side: pink lines represent hydrogen bonding interactions, green lines represent the pi–pi stacking interactions while red lines signify cation–pi stacking interactions).

favourable bonded and non-interactions with the active site of hSERT. The detailed representations are given in Fig. 1S–12S.† Fig. 6 shows the binding mode of **13c** into the active site of

Human Serotonin Transporter, where pink lines represent hydrogen bonding interactions, green lines indicate π–π stacking interactions, and red lines signify cation–π stacking

interactions. Overall, the *in silico* study suggests that chalcone derivatives could accommodate well into the active site of hSERT and thus could serve as a pertinent starting point for fragmented-based optimization to arrive at potent leads targeting hSERT.

2.5. DFT study

The optimized molecular structure and molecular electrostatic surface potential (MESP) of compound **13c** were obtained using the DFT method at the B3LYP/6-31G(d,p) level (Fig. 7). The optimized structure reveals a stable conformation with well-balanced bond lengths and angles, consistent with the expected values for similar heterocyclic compounds. The presence of conjugation and electron delocalization across the enone, pyrazole, benzotriazole and carbazole moieties contributes to the molecule's structural stability and potential biological activity. The planarity of the conjugated system and the substitution pattern suggest that π–π stacking interactions may play a significant role in antidepressant activity. The MESP map highlights the charge distribution across the molecule, indicating regions of high electron density (red) around the oxygen and nitrogen atoms, which are likely to act as nucleophilic centers for intermolecular interactions.[61] The low electron density regions (blue) around hydrogen atoms and aromatic rings suggest potential electrophilic sites for receptor interactions, while the moderate electron density areas (yellow and green) indicate possible van der Waals forces and π–π stacking interactions.[62] This distinct charge distribution pattern suggests a balanced hydrophilic and hydrophobic character, which may enhance membrane permeability and receptor binding efficiency. The combined structural and electrostatic
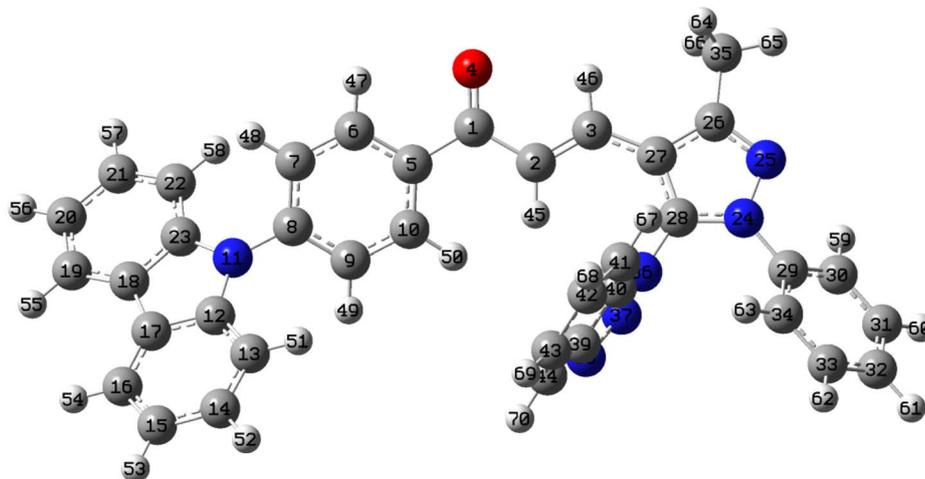
Optimized molecular structure of compound 13c
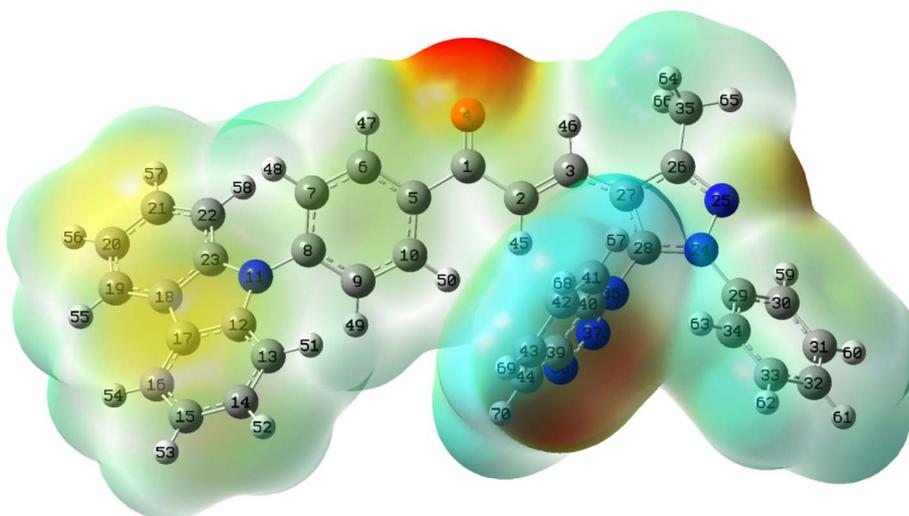
Molecular electrostatic surface potential of compound 13c

Fig. 7 Optimized molecular structure and molecular electrostatic surface potential of the compound **13c** was obtained using the DFT method at the B3LYP/6-31G(d,p) level.

analysis confirms that compound **13c** possesses favorable conformational stability and electronic properties, which are essential for its potential pharmacological activity. The bond length data of the compound **13c** was obtained using the DFT method at the B3LYP/6-31G(d,p) level (Table 2S†). The calculated bond lengths provide detailed insights into the molecular geometry and electronic structure of the compound. The C–C bond lengths in the aromatic rings fall in the expected range of 1.38–1.42 Å, indicating delocalized π-electron density within the rings. Notably, the C1–O4 bond length of 1.231 Å is consistent with the presence of a carbonyl group, suggesting partial double-bond character due to conjugation with the adjacent π-system. The C8–N11 bond length of 1.416 Å reflects the partial double-bond nature of the pyrazole nitrogen, which is in line with the electron-donating effect of the nitrogen atom. The N24–N25 bond length of 1.360 Å and the N36–N37 bond length of 1.391 Å are indicative of single bond character, suggesting minimal delocalization of electron density between these nitrogen atoms. The C17–C18 bond length of 1.448 Å is longer than typical aromatic C–C bonds, which could be attributed to steric hindrance or electronic effects within the conjugated system. The bond lengths involving hydrogen atoms, such as C–H and N–H bonds, are in the range of 1.082–1.095 Å, which is consistent with expected values for sp² hybridized carbon and nitrogen atoms. The DFT-based bond length analysis of **13c** reveals extensive conjugation and electronic delocalization across the molecule. The bond length pattern supports the aromatic character of the pyrazole, benzotriazole, and carbazole rings, as well as the conjugated nature of the α,β-unsaturated ketone moiety. This electronic structure may enhance the molecule's chemical stability and biological activity, making it a promising candidate for further medicinal chemistry optimization.

2.6. ADME and pharmacokinetics profile

The ADME (Absorption, Distribution, Metabolism, and Excretion) characteristics of the synthesized compounds (**13a–13d**, **14a–14d**, and **15a–15d**) were comprehensively analyzed using the SwissADME tool.[63] to determine their suitability as potential drug candidates (Tables 7 and 1S†). Compound **13c** had the highest number of aromatic heavy atoms (39), indicating strong π–π interactions that might improve membrane permeability but decrease water solubility. All compounds displayed 6 rotatable bonds, suggesting uniform molecular flexibility that could facilitate receptor binding while potentially limiting oral bioavailability. The number of hydrogen bond acceptors ranged from 2 to 4, with no hydrogen bond donors, consistent with Lipinski's rule. Molar refractivity values were elevated in the 13-series (up to 175.10 for **13c**), signifying higher polarizability,

Table 7 ADME properties of synthesized compounds including physicochemical properties, lipophilicity, water solubility, pharmacokinetics and drug-likeness using the SwissADME tool

Parameter	13a	13b	13c	13d	14a	14b	14c	14d	15a	15b	15c	15d
Physicochemical properties												
Num. Heavy atoms	41	41	44	37	37	37	40	33	33	33	36	29
Num. arom. Heavy atoms	30	30	39	30	26	26	35	26	22	22	31	22
Num. rotatable bonds	6	6	6	6	6	6	6	6	6	6	6	6
Num. H-bond acceptors	2	3	4	3	2	3	4	3	2	3	4	3
Num. H-bond donors	0	0	0	0	0	0	0	0	0	0	0	0
Molar refractivity	172.12	168.40	175.10	149.17	154.62	150.90	157.59	131.66	137.11	133.39	140.09	114.16
TPSA (Å²)	43.06	52.29	70.53	49.05	43.06	52.29	70.53	49.05	43.06	52.29	70.53	49.05
Lipophilicity												
Consensus log $P_{o/w}$	6.66	5.82	6.62	6.07	5.77	4.92	5.66	5.12	4.82	3.97	4.73	4.16
Water solubility												
Log S (ESOL)	−8.63	−7.87	−8.88	−7.73	−7.82	−6.75	−8.28	−6.91	−6.27	−5.52	−6.55	−5.38
Pharmacokinetics												
GI absorption	Low	High	Low	Low	High	High	High	High	High	High	High	High
BBB permeant	No	No	No	No	No	Yes	No	No	Yes	Yes	No	Yes
P-gp substrate	No	No	No	No	No	No	No	No	Yes	Yes	No	No
CYP1A2 inhibitor	No	No	No	No	No	No	No	No	No	No	No	Yes
CYP2C19 inhibitor	Yes	Yes	No	Yes	Yes	Yes	No	Yes	Yes	Yes	No	Yes
CYP2C9 inhibitor	No	No	No	No	No	Yes	No	Yes	Yes	Yes	Yes	Yes
CYP2D6 inhibitor	Yes	No	No	No	No	No	No	No	No	No	No	No
CYP3A4 inhibitor	No	No	No	No	No	No	No	No	Yes	No	No	No
Drug-likeness												
Lipinski violations	2	2	2	1	2	0	2	1	0	0	1	0
Ghose violations	4	4	3	3	3	2	3	2	1	1	1	0
Veber rule	Yes	Yes	Yes	Yes	Yes	Yes	Yes	Yes	Yes	Yes	Yes	Yes
Egan rule	No	No	No	No	No	Yes	No	No	Yes	Yes	Yes	Yes
Muegge rule	No	No	No	No	No	No	No	No	No	No	No	Yes

which may strengthen target binding but reduce solubility. TPSA values spanned from 43.06 $Å^2$ to 70.53 $Å^2$, with most compounds falling within the optimal range for passive membrane permeability. Lipophilicity, assessed *via* consensus log $P_{o/w}$, ranged from 3.97 to 6.66; the 13-series was more lipophilic, potentially enhancing membrane permeability but negatively impacting aqueous solubility and metabolic stability. Water solubility (log S) was generally poor, with values between −5.38 and −8.88, particularly for the highly aromatic 13-series. Pharmacokinetic analysis indicated high gastrointestinal (GI) absorption for most 14-series and 15-series compounds, whereas the 13-series showed low GI absorption, likely due to larger molecular size and increased lipophilicity. Blood–brain barrier (BBB) permeability was noted for **14b**, **15a**, **15b**, and **15d**, hinting at possible CNS activity but also raising concerns about CNS-related side effects. P-glycoprotein (P-gp) substrate interaction was predicted only for **15a** and **15b**, suggesting potential drug efflux and lower bioavailability. CYP enzyme inhibition studies revealed selective inhibition of CYP2C19 and CYP2C9 by several compounds, with minimal inhibition of CYP1A2, CYP2D6, and CYP3A4, indicating a reduced risk of metabolic interactions. Drug-likeness analysis showed that 15-series compounds best adhered to Lipinski's rule and met Egan and Muegge criteria, indicating balanced properties. Most compounds violated the Ghose rule due to high molecular weight and refractivity, but Veber rule compliance suggested good oral bioavailability.

3 Materials and methods

3.1. Chemicals and instrumentations

All chemicals and solvents used in this study were of analytical grade and were used without further purification. Carbazole (≥95%, Sigma-Aldrich), indole (≥99%, TCI), pyrrole (≥97%, Sigma-Aldrich), 4-fluoroacetophenone (≥99%, Sigma-Aldrich), ethyl acetoacetate (≥99%), phenylhydrazine (≥98%, Avra Synthesis), phosphoryl chloride (POCl₃, 98%, Avra Synthesis), dimethylformamide (DMF, ≥99% Avra Synthesis), potassium carbonate (K₂CO₃, ≥98%, Avra Synthesis), methanol (≥99.5%, TCI), and sodium hydride (NaH, 57–63%%, Avra Synthesis) were purchased. The solvents such as ethanol (≥99.5%), hexane (≥95%), and ethyl acetate (≥99%) were obtained from local vendor. All reactions were carried out under an inert nitrogen atmosphere unless otherwise specified. Thin-layer

chromatography (TLC) was performed using silica gel 60 F₂₅₄ plates (Merck) and visualized under UV light at 254 nm and 365 nm. Nuclear Magnetic Resonance (NMR) spectra were recorded using a BRUKER AVANCE III HD NMR 500 MHz spectrometer (liquid state) with tetramethylsilane (TMS) as the internal standard and CDCl₃ as a solvent. Fourier-transform infrared (FT-IR) spectra were obtained using a BRUKER FT-IR spectrometer. Melting points were determined using an open capillary method and are uncorrected.

3.2. Experimental procedures

3.2.1. Synthesis of 1-(4-(9H-carbazol-9-yl)phenyl)ethan-1-one (3).
To a stirred solution of NaH (11 mmol) in dry DMF (15 mL), carbazole (**1**, 10 mmol) was added dropwise under an inert atmosphere. Subsequently, 4-fluoroacetophenone (**2**, 10 mmol) was introduced into the mixture, and the reaction mixture was transferred to a pressure reactor. The temperature was gradually raised to 230 °C and maintained for 12 hours. The progress of the reaction was monitored by TLC using a mobile phase of ethyl acetate and *n*-hexane (1 : 9). Upon completion of the reaction, the mixture was cooled to room temperature and quenched with methanol. The reaction mass was then poured into cold water, and the resulting precipitate was filtered, thoroughly washed with water, and dried. The crude product was purified by recrystallization from methanol, yielding compound **3** with 92% purity. The compound **3** was characterized using NMR spectroscopy. The synthesis of compound **3** is depicted in Scheme 2.

3.2.2. Synthesis of 1-(4-(1H-indol-1-yl)phenyl)ethan-1-one (5).
To a stirred solution of NaH (11 mmol) in DMF (15 mL), indole (**4**, 10 mmol) was added dropwise under an inert atmosphere. To this mixture, 4-fluoroacetophenone (**2**, 10 mmol) was added, and the reaction mixture was heated in an oil bath at 110–115 °C for 4 hours. Upon completion of the reaction, as monitored by TLC (1 : 9 ethyl acetate : hexane), the mixture was allowed to cool to room temperature and subsequently quenched with methanol. The reaction mass was poured into cold water, and the resulting precipitate was filtered, washed with water, and dried. The crude product was purified by recrystallization using methanol to yield 90% pure compound **5**. The compound **5** was characterized using NMR spectroscopy. The synthesis of compound **5** is depicted in Scheme 3.
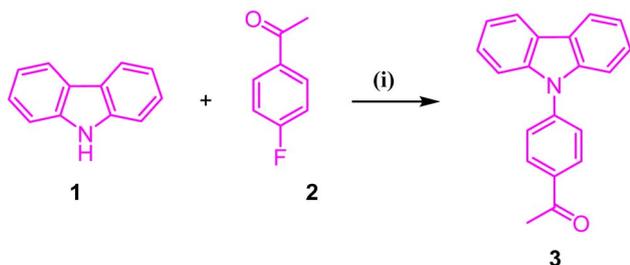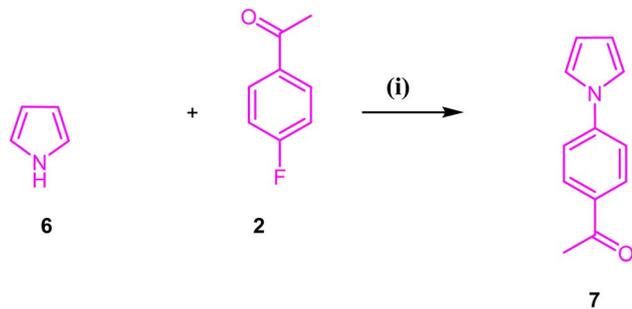

Scheme 2 Synthesis of 1-(4-(9H-carbazol-9-yl)phenyl)ethan-1-one (**3**). (i) NaH, dry DMF, 230 °C, 12 h, pressure reactor.
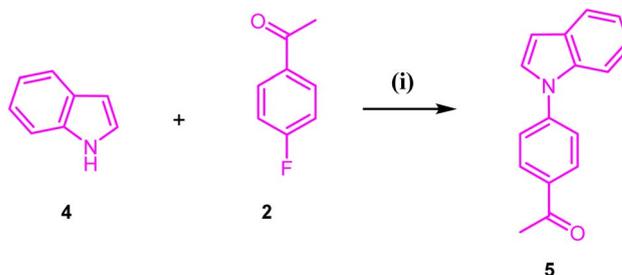
Scheme 3 Synthesis of 1-(4-(1H-indol-1-yl)phenyl)ethan-1-one (**5**). (i) NaH, dry DMF, 110–115 °C, 4 h.

Scheme 4 Synthesis of 1-(4-(1H-pyrrol-1-yl)phenyl)ethan-1-one (**7**). (i) NaH, dry DMF, 0–5 °C, 2 h, rt, 2 h.

3.2.3. Synthesis of 1-(4-(1H-pyrrol-1-yl)phenyl)ethan-1-one. To a stirred solution of NaH (11 mmol) in DMF (15 mL) at 0 °C, pyrrole (**6**, 10 mmol) was added dropwise under an inert atmosphere. The reaction mixture was cooled to 0–5 °C, and 4-fluoroacetophenone (**2**, 10 mmol) was added slowly. The reaction mixture was stirred at the same temperature for 2 hours, followed by stirring at room temperature for an additional 2 hours. Upon completion of the reaction, as monitored by TLC (1 : 9 ethyl acetate : hexane), the mixture was allowed to cool to room temperature and subsequently quenched with methanol. The reaction mass was then poured into cold water, and the resulting precipitate was filtered, washed with water, and dried. The crude product was purified by recrystallization using methanol, yielding 85% of pure compound **7**. The compound **7** was characterized using NMR spectroscopy. The synthesis of compound **7** is depicted in Scheme 4.

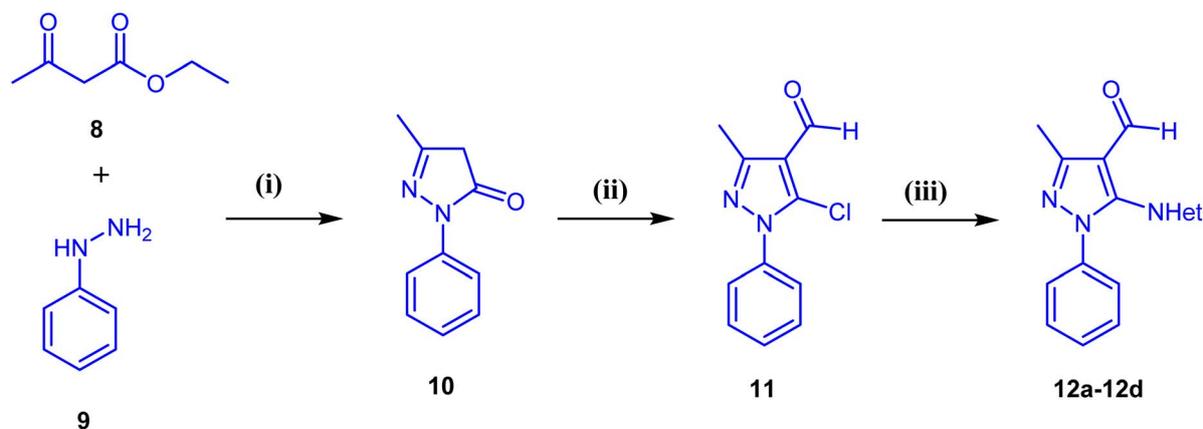**3.2.4. Synthesis of 3-methyl-1-phenyl-5-(heterocyclic substituted)-1H-pyrazole-4-carbaldehydes (12a–12d).** Compounds **10**, **11** and **12a–12d** were synthesized following a previously reported method.[64] Ethyl acetoacetate (**8**, 200 mmol) and phenyl hydrazine (**9**, 200 mmol) were reacted in ethanol (10 mL) at 60–70 °C to yield 5-methyl-2-phenyl-2,4-dihydro-3H-pyrazol-3-one (**10**). For the synthesis of compound **11**, DMF (300 mmol) was first cooled, and POCl$_3$ (700 mmol) was

added dropwise under controlled conditions. To this ice-cold mixture, compound **3**, (100 mmol) was added, and the resulting reaction mixture was refluxed until the formation of the desired product was confirmed by TLC. The reaction mixture was then poured onto ice-cold water, and the crude product was filtered, dried, and recrystallized to obtain 5-chloro-3-methyl-1-phenyl-1H-pyrazole-4-carbaldehyde (**11**) as white crystals. Following this, carbaldehydes (**12a–12d**), in a 50 mL round-bottom flask equipped with a mechanical stirrer and condenser, carbaldehyde **4** (10 mmol), piperidine or morpholine or benzotriazole or imidazole (12 mmol), and anhydrous K$_2$CO$_3$ (20 mmol) were combined in DMF (20 mL). The reaction mixture was refluxed until the formation of the product was confirmed by TLC. Upon completion, the mixture was cooled to room temperature and poured into ice-cold water with continuous stirring. The solution was then neutralized with 1 N HCl until a pH of 7 was achieved. The desired products (**12a–12d**), were separated, thoroughly washed with water, dried, and recrystallized from hot ethanol to obtain the final compounds. The compounds **12a–12d** were characterized using NMR spectroscopy. The detailed synthesis is depicted in Scheme 5.
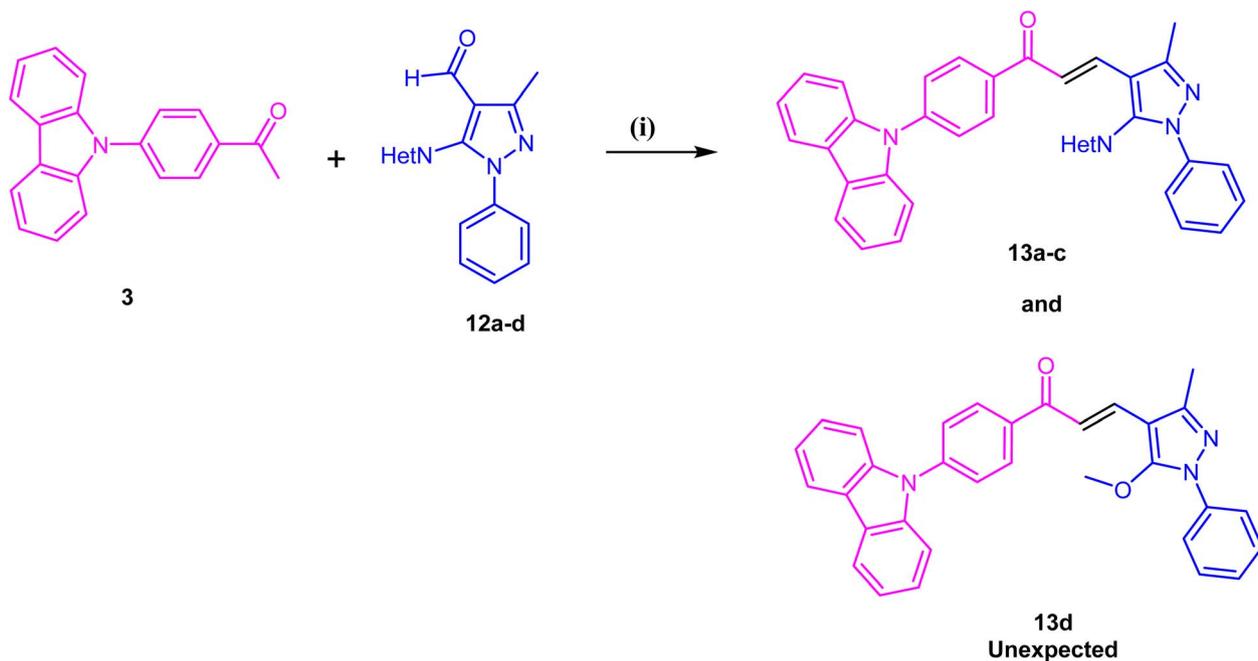
3.2.5. Synthesis of chalcones-

3.2.5.1. Synthesis of chalcones (13a–13d). A mixture of 1-(4-(9H-carbazol-9-yl)phenyl)ethan-1-one (**3**, 5 mmol) and 3-methyl-1-phenyl-5-(heterocyclic substituted)-1H-pyrazole-4-carbaldehydes (**12a–12d**, 5.5 mmol) were dissolved in methanol (10 mL). KOH (7.5 mmol) was added, and the reaction mixture was refluxed for 8–10 hours. After completion of the reaction, monitored by TLC, the mixture was cooled to room temperature. The solid product was filtered, washed with cold methanol, and dried at 60 °C. The crude product was purified using methanol to afford the desired compounds **13a–13c** and the unexpected compound **13d**. The compounds **13a–13d** were characterized using FT-IR, ^{1}H NMR, ^{13}C NMR and mass spectral methods. The detailed synthesis is depicted in Scheme 6.

3.2.5.2. Synthesis of chalcones (14a–14d). A mixture of 1-(4-(1H-indol-1-yl)phenyl)ethan-1-one (**5**, 5 mmol) and 3-methyl-1-phenyl-5-(heterocyclic substituted)-1H-pyrazole-4-

Scheme 5 Synthesis of 3-methyl-1-phenyl-5-(heterocyclic substituted)-1H-pyrazole-4-carbaldehydes (**12a–12d**). Where −NHet = piperidinyl, morpholinyl, imidazolyl and benzotriazolyl. (i) EtOH, 60–70 °C; (ii) POCl$_3$, DMF, reflux; (iii) Piperidine/Morpholine/Benzotriazole/Imidazole, K$_2$CO$_3$, DMF, reflux.
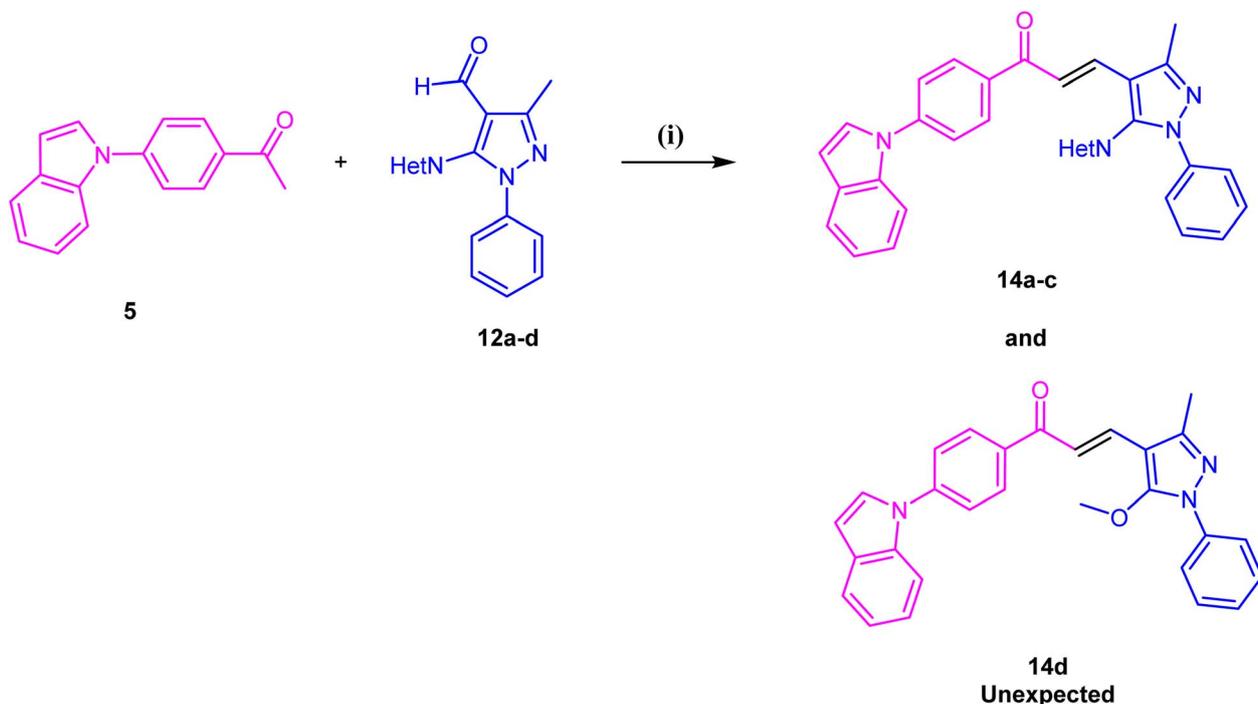
Scheme 6 Synthesis of chalcones by combining 3-methyl-1-phenyl-5-(heterocyclic substituted)-1*H*-pyrazole-4-carbaldehyde and 1-(4-(9*H*-carbazol-9-yl)phenyl)ethan-1-one. Where −NHet = piperidinyl, morpholinyl, imidazolyl and benzotriazolyl. (i) MeOH, KOH, reflux, 8–10 h.

carbaldehydes (**12a–12d**, 5.5 mmol) were dissolved in methanol (10 mL). Potassium hydroxide (KOH) (7.5 mmol) was added, and the reaction mixture was heated at 50 °C under reflux for 6 hours. After completion of the reaction, monitored by thin-layer chromatography (TLC), the mixture was cooled to room temperature. The solid product was filtered, washed with cold methanol, and dried at 60 °C. The crude product was purified using methanol to afford the desired compounds **14a–14c** and

Scheme 7 Synthesis of chalcones by combining 3-methyl-1-phenyl-5-(heterocyclic substituted)-1*H*-pyrazole-4-carbaldehyde and 1-(4-(1*H*-indol-1-yl)phenyl)ethan-1-one. Where −NHet = piperidinyl, morpholinyl, imidazolyl and benzotriazolyl. (i)MeOH, KOH, reflux, 6 h.
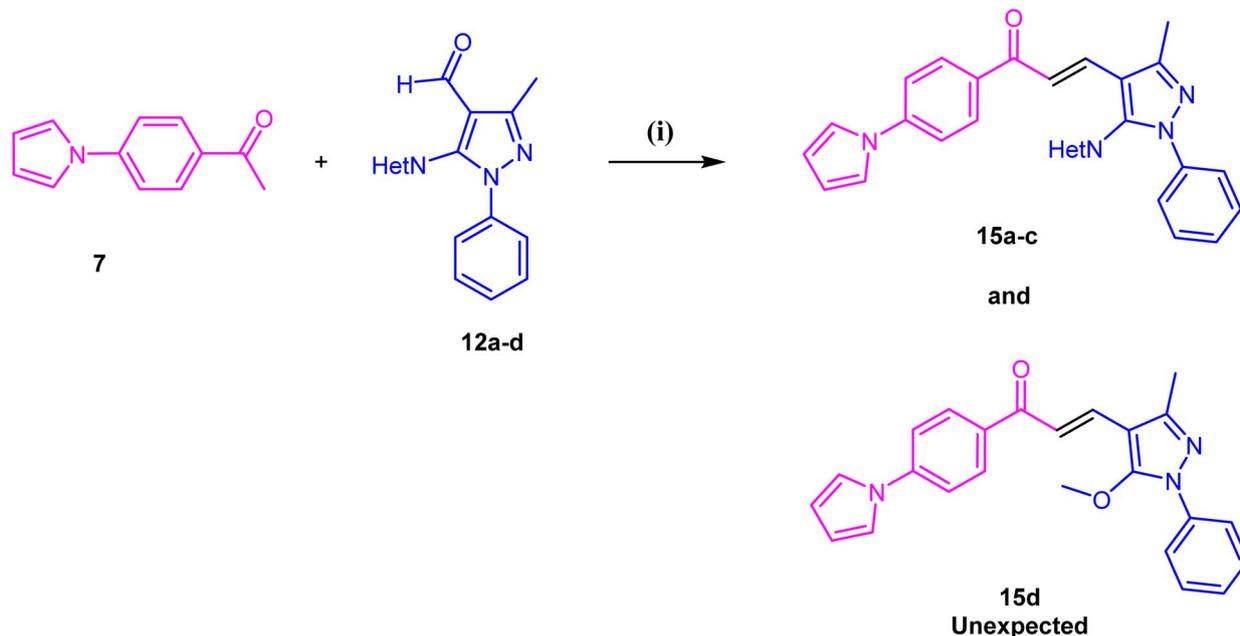
Scheme 8 Synthesis of chalcones by combining 3-methyl-1-phenyl-5-(heterocyclic substituted)-1*H*-pyrazole-4-carbaldehydes and 1-(4-(1*H*-pyrrol-1-yl)phenyl)ethan-1-one. Where −NHet = piperidinyl, morpholinyl, imidazolyl and benzotriazolyl. (i) MeOH, KOH, reflux, 6 h.

the unexpected compound **14d**. The compounds **14a–14d** were characterized using FT-IR, ^{1}H NMR, ^{13}C NMR and mass spectral methods. The detailed synthesis is depicted in Scheme 7.

3.2.5.3. Synthesis of chalcones (15a–15d). A mixture of 1-(4-(1*H*-pyrrol-1-yl)phenyl)ethan-1-one (**7**, 5 mmol) and 3-methyl-1-phenyl-5-(heterocyclic substituted)-1*H*-pyrazole-4-carbaldehydes (**12a–12d**, 5.5 mmol) were dissolved in methanol (10 mL). KOH (7.5 mmol) was added, and the reaction mixture was heated at 50 °C under reflux for 6 hours. After completion of the reaction, monitored by TLC, the mixture was cooled to room temperature. The solid product was filtered, washed with cold methanol, and dried at 60 °C. The crude product was purified using methanol as to afford the desired compounds **15a–15c** and the unexpected compound **15d**. The compounds **15a–15d** were characterized using FT-IR, ^{1}H NMR, ^{13}C NMR and mass spectral methods. The detailed synthesis is depicted in Scheme 8.

3.3. Spectral data of the synthesized compounds

3.3.1. 1-(4-(9*H*-Carbazol-9-yl)phenyl)ethan-1-one (3). Creamy solid; m.p. 208–210 °C; ^{1}H NMR (500 MHz, CDCl$_3$, δ): 8.21 (d, J = 8.6 Hz, 2H), 8.15 (d, J = 8.0 Hz, 2H), 7.71 (d, J = 8.6 Hz, 2H), 7.48 (d, J = 8.0 Hz, 2H), 7.45–7.41 (m, 2H), 7.34–7.30 (m, 2H), 2.70 (s, 3H); ^{13}C NMR (126 MHz, CDCl$_3$, δ): 197.00, 142.20, 140.23, 135.54, 130.15, 126.51, 126.24, 123.87, 120.65, 120.50, 109.79, 26.72.

3.3.2. 1-(4-(1*H*-Indol-1-yl)phenyl)ethan-1-one (5). White solid; m.p. 84–86 °C; ^{1}H NMR (500 MHz, CDCl$_3$, δ): 8.13 (d, J = 8.7 Hz, 2H), 7.70 (d, J = 7.8 Hz, 1H), 7.66–7.61 (m, 3H), 7.38 (d, J = 3.3 Hz, 1H), 7.28 (dd, J = 7.1, 1.1 Hz, 1H), 7.22–7.18 (m, 1H), 6.74 (m, 1H), 2.66 (s, 3H); ^{13}C NMR (126 MHz, CDCl$_3$, δ): 196.83,

143.80, 135.39, 134.55, 130.06, 129.83, 127.34, 123.29, 122.92, 121.42, 121.03, 110.57, 105.06, 26.59.

3.3.3. 1-(4-(1*H*-Pyrrol-1-yl)phenyl)ethan-1-one (7). White solid; m.p. 118–120 °C; ^{1}H NMR (500 MHz, CDCl$_3$, δ): 8.03 (d, J = 8.6 Hz, 2H), 7.47 (d, J = 8.6 Hz, 2H), 7.20–7.13 (m, 2H), 6.43–6.35 (m, 2H), 2.62 (s, 3H); ^{13}C NMR (126 MHz, CDCl$_3$, δ): 196.77, 144.05, 134.03, 130.20, 119.36, 119.02, 111.64, 26.53.

3.3.4. 3-Methyl-1-phenyl-5-(piperidin-1-yl)-1*H*-pyrazole-4-carbaldehyde (12a). Faint yellow solid; m.p. 115–117 °C; ^{1}H NMR (500 MHz, CDCl$_3$, δ): 10.01 (s, 1H), 7.55–7.51 (m, 2H), 7.48–7.44 (m, 2H), 7.39–7.35 (m, 1H), 3.11 (s, 4H), 2.46 (s, 3H), 1.55 (s, 6H); ^{13}C NMR (126 MHz, CDCl$_3$, δ): 183.67, 153.94, 151.79, 139.46, 129.14, 127.96, 124.74, 112.18, 52.40, 25.80, 23.70, 14.12.

3.3.5. 3-Methyl-5-morpholino-1-phenyl-1*H*-pyrazole-4-carbaldehyde (12b). Faint yellow solid; m.p. 135–137 °C; ^{1}H NMR (500 MHz, CDCl$_3$, δ): 9.98 (s, 1H), 7.52–7.47 (m, 4H), 7.42–7.39 (m, 1H), 3.70–3.68 (m, 4H), 3.16–3.14 (m, 4H), 2.47 (s, 3H); ^{13}C NMR (126 MHz, CDCl$_3$, δ): 183.24, 152.30, 151.76, 139.08, 129.29, 128.41, 124.98, 112.09, 66.78, 50.88, 13.63.

3.3.6. 5-(1*H*-Benzo[*d*][1,2,3]triazol-1-yl)-3-methyl-1-phenyl-1*H*-pyrazole-4-carbaldehyde (12c). Yellow solid; m.p. 236–238 °C; ^{1}H NMR (500 MHz, CDCl$_3$, δ): 9.69 (s, 1H), 8.14 (dt, J = 8.2, 1.0 Hz, 1H), 7.49–7.44 (m, 2H), 7.26–7.21 (m, 3H), 7.21–7.19 (m, 1H), 7.17–7.15 (m, 2H), 2.71 (s, 3H); ^{13}C NMR (126 MHz, CDCl$_3$, δ): 183.40, 151.64, 145.37, 136.83, 136.80, 133.98, 129.72, 129.49, 129.09, 125.20, 123.51, 120.70, 116.79, 109.26, 13.90.

3.3.7. 5-(1*H*-Imidazol-1-yl)-3-methyl-1-phenyl-1*H*-pyrazole-4-carbaldehyde (12d). Yellow solid; m.p. 204–206 °C; ^{1}H NMR (500 MHz, CDCl$_3$, δ): 9.78 (s, 1H), 7.60 (s, 1H), 7.40–7.38 (m, 3H), 7.23–7.22 (m, 1H), 7.16–7.14 (m, 2H), 7.03 (t, J = 1.3 Hz, 1H), 2.62 (s, 3H); ^{13}C NMR (126 MHz, CDCl$_3$, δ): 183.20, 151.37,

138.33, 137.84, 136.54, 131.05, 129.70, 129.13, 123.36, 120.60, 115.39, 13.73.

3.3.8. (E)-1-(4-(9H-Carbazol-9-yl)phenyl)-3-(3-methyl-1-phenyl-5-(piperidin-1-yl)-1H-pyrazol-4-yl)prop-2-en-1-one (13a).

Faint yellow solid; m.p. 197–200 °C; FT-IR (cm^{-1}): 3052.33, 2928.02, 2826.89, 1657.09, 1589.00, 1500.06, 1442.99, 1382.68, 1337.97, 1284.79, 1253.54, 1215.80, 1164.32, 1106.85, 1072.18, 1029.38, 1004.09, 911.28, 856.91, 828.95, 797.41, 746.42, 726.45, 696.12, 638.77, 564.06, 524.18; ^{1}H NMR (500 MHz, CDCl$_3$, δ): 8.25 (d, J = 8.5 Hz, 2H), 8.16 (m, 2H), 8.11 (d, J = 15.6 Hz, 1H), 7.75 (d, J = 8.5 Hz, 2H), 7.57–7.42 (m, 8H), 7.39–7.28 (m, 4H), 3.20–3.03 (m, 4H), 2.54 (s, 3H), 1.61–1.56 (m, 6H); ^{13}C NMR (126 MHz, CDCl$_3$, δ): 189.33, 152.13, 148.92, 141.41, 140.32, 139.62, 137.40, 137.01, 130.01, 129.19, 129.01, 127.78, 126.56, 126.16, 124.80, 124.37, 123.78, 120.50, 120.44, 117.55, 109.80, 108.90, 26.17, 23.83, 15.62; HRMS (ESI, M + H): for C$_{36}$H$_{32}$N$_4$O, calculated: 537.2654, observed: 537.2663.

3.3.9. (E)-1-(4-(9H-Carbazol-9-yl)phenyl)-3-(3-methyl-5-morpholino-1-phenyl-1H-pyrazol-4-yl)prop-2-en-1-one (13b).

Yellow solid; m.p. 204–207 °C; FT-IR (cm^{-1}): 3052.79, 2960.81, 2830.00, 1681.46, 1628.89, 1592.13, 1536.62, 1501.60, 1441.31, 1359.84, 1272.02, 1226.86, 1165.14, 1104.52, 1067.55, 1006.18, 974.10, 918.19, 843.40, 753.37, 687.85, 632.08, 593.08, 567.00, 534.40; ^{1}H NMR (500 MHz, CDCl$_3$, δ): 8.26 (d, J = 8.4 Hz, 2H), 8.16 (d, J = 7.7 Hz, 2H), 8.08 (d, J = 15.6 Hz, 1H), 7.76 (d, J = 8.4 Hz, 2H), 7.57–7.31 (m, 12H), 3.78–3.71 (m, 4H), 3.18–3.12 (m, 4H), 2.55 (s, 3H), 1.58 (s, 2H); ^{13}C NMR (126 MHz, CDCl$_3$, δ): 188.96, 150.29, 148.95, 141.62, 140.27, 139.29, 137.11, 136.07, 130.02, 129.18, 128.23, 126.58, 126.19, 125.04, 123.80, 120.55, 120.44, 118.38, 109.80, 109.38, 67.05, 50.99, 15.48; MS (M + H): for C$_{35}$H$_{30}$N$_4$O$_2$, calculated: 539.2447, observed: 539.2795.

3.3.10. (E)-3-(5-(1H-Benzo[d][1,2,3]triazol-1-yl)-3-methyl-1-phenyl-1H-pyrazol-4-yl)-1-(4-(9H-carbazol-9-yl)phenyl)prop-2-en-1-one (13c).

Off white solid; m.p. 185–187 °C; FT-IR (cm^{-1}): 3055.16, 2102.71, 1787.51, 1660.53, 1596.63, 1509.11, 1442.59, 1390.69, 1349.02, 1325.63, 1275.14, 1216.59, 1161.64, 1022.15, 970.12, 830.85, 794.16, 747.28, 688.15, 627.66, 564.23, 527.34; ^{1}H NMR (500 MHz, CDCl$_3$, δ): 8.17 (m, 3H), 7.81 (d, J = 8.4 Hz, 2H), 7.65–7.58 (m, 3H), 7.52 (t, J = 7.4 Hz, 1H), 7.44 (m, 4H), 7.32 (m, 2H), 7.23 (m, 7H), 6.71 (d, J = 15.9 Hz, 1H), 2.71 (s, 3H); ^{13}C NMR (126 MHz, CDCl$_3$, δ): 188.14, 150.38, 145.57, 141.97, 140.18, 137.24, 136.04, 133.84, 132.20, 131.92, 130.00, 129.77, 129.43, 128.67, 126.46, 126.23, 125.20, 123.85, 123.30, 121.82, 120.73, 120.64, 120.47, 114.89, 109.81, 109.49, 13.94; MS (M + H): for C$_{37}$H$_{26}$N$_6$O, calculated: 571.2246, observed: 571.2750.

3.3.11. (E)-1-(4-(9H-Carbazol-9-yl)phenyl)-3-(5-methoxy-3-methyl-1-phenyl-1H-pyrazol-4-yl)prop-2-en-1-one (13d).

Light tan solid; m.p. 190–193 °C; FT-IR (cm^{-1}): 3052.32, 1656.13, 1588.56, 1506.26, 1479.93, 1446.36, 1405.86, 1333.32, 1258.44, 1221.50, 1168.03, 1026.86, 975.63, 829.19, 748.34, 717.02, 698.32, 647.26, 564.03, 520.97; ^{1}H NMR (500 MHz, CDCl$_3$, δ): 8.27 (d, J = 7.9 Hz, 2H), 8.16 (d, J = 7.9 Hz, 2H), 7.90 (d, J = 15.6 Hz, 1H), 7.74 (m, 4H), 7.47 (m, 7H), 7.34 (m, 3H), 3.91 (s, 3H), 2.51 (s, 3H); ^{13}C NMR (126 MHz, CDCl$_3$, δ): 189.06, 154.29, 149.40, 141.70, 140.31, 137.80, 137.10, 134.70, 130.11, 129.33, 127.44, 126.60, 126.22, 123.84, 122.39, 120.58, 120.48, 118.59,

109.84, 104.50, 61.96, 14.48; HRMS (ESI, M + H): for C$_{32}$H$_{25}$N$_3$O$_2$, calculated: 484.2025, observed: 484.2026.

3.3.12. (E)-1-(4-(1H-Indol-1-yl)phenyl)-3-(3-methyl-1-phenyl-5-(piperidin-1-yl)-1H-pyrazol-4-yl)prop-2-en-1-one (14a).

Faint yellow solid; m.p. 154–157 °C; FT-IR (cm^{-1}): 3054.34, 2940.96, 2818.25, 1654.72, 1586.40, 1499.29, 1446.35, 1383.26, 1342.22, 1285.55, 1258.45, 1215.41, 1172.05, 1123.81, 1070.75, 1016.98, 996.33, 953.30, 917.38, 828.37, 798.16, 736.49, 687.83, 646.06, 599.41, 569.60, 522.65; ^{1}H NMR (500 MHz, CDCl$_3$, δ): 8.18 (d, J = 8.5 Hz, 2H), 8.08 (d, J = 15.6 Hz, 1H), 7.72–7.64 (m, 4H), 7.55 (d, J = 7.6 Hz, 2H), 7.47 (t, J = 7.8 Hz, 2H), 7.43–7.35 (m, 2H), 7.28 (m, 2H), 7.21 (t, J = 7.3 Hz, 1H), 6.74 (d, J = 3.1 Hz, 1H), 3.09 (m, 4H), 2.53 (s, 3H), 1.58 (s, 6H); ^{13}C NMR (126 MHz, CDCl$_3$, δ): 189.04, 152.09, 148.92, 143.22, 139.66, 136.75, 136.38, 135.50, 129.98, 129.81, 129.03, 127.79, 127.47, 124.83, 123.47, 122.88, 121.41, 120.97, 117.50, 110.66, 108.94, 104.91, 52.26, 26.18, 23.86, 15.60; MS (M + H): for C$_{32}$H$_{30}$N$_4$O, calculated: 487.2497, observed: 487.2866.

3.3.13. (E)-1-(4-(1H-Indol-1-yl)phenyl)-3-(3-methyl-5-morpholino-1-phenyl-1H-pyrazol-4-yl)prop-2-en-1-one (14b).

Yellow solid; m.p. 177–180 °C; FT-IR (cm^{-1}): 3056.11, 2980.09, 2900.23, 2858.86, 1658.83, 1589.81, 1494.53, 1443.33, 1373.23, 1336.57, 1277.86, 1212.53, 1171.63, 1107.49, 1073.81, 1004.26, 919.36, 871.66, 837.40, 802.07, 745.45, 690.15, 650.49, 578.31, 519.48; ^{1}H NMR (500 MHz, CDCl$_3$, δ): 8.19 (d, J = 8.5 Hz, 2H), 8.05 (d, J = 15.6 Hz, 1H), 7.73–7.64 (m, 4H), 7.55 (d, J = 7.6 Hz, 2H), 7.49 (t, J = 7.7 Hz, 2H), 7.43–7.37 (m, 2H), 7.33 (d, J = 15.6 Hz, 1H), 7.28 (d, J = 7.3 Hz, 1H), 7.21 (t, J = 7.4 Hz, 1H), 6.75 (d, J = 3.1 Hz, 1H), 3.76–3.68 (m, 4H), 3.17–3.10 (m, 4H), 2.54 (s, 3H); ^{13}C NMR (126 MHz, CDCl$_3$, δ): 188.76, 150.26, 148.96, 143.40, 139.33, 136.11, 135.87, 135.48, 130.01, 129.83, 129.20, 128.25, 127.44, 125.08, 123.48, 122.92, 121.43, 121.02, 118.39, 110.66, 109.41, 105.00, 67.08, 51.00, 15.46; MS (M + H): for C$_{31}$H$_{28}$N$_4$O$_2$, calculated: 489.2290, observed: 487.2866.

3.3.14. (E)-3-(5-(1H-Benzo[d][1,2,3]triazol-1-yl)-3-methyl-1-phenyl-1H-pyrazol-4-yl)-1-(4-(1H-indol-1-yl)phenyl)prop-2-en-1-one (14c).

Off white solid; m.p. 171–174 °C; FT-IR (cm^{-1}): 3084.49, 1659.45, 1593.63, 1512.39, 1450.15, 1403.41, 1343.51, 1281.95, 1215.03, 1173.45, 1131.52, 1078.94, 1032.81, 956.02, 919.40, 875.29, 832.34, 744.95, 687.07, 569.03; ^{1}H NMR (500 MHz, CDCl$_3$, δ): 8.19 (d, J = 8.3 Hz, 1H), 7.75 (d, J = 8.5 Hz, 2H), 7.69 (d, J = 7.8 Hz, 1H), 7.59 (m, 2H), 7.51 (m, 3H), 7.45 (t, J = 7.4 Hz, 1H), 7.35 (d, J = 3.3 Hz, 1H), 7.27–7.20 (m, 8H), 6.73 (d, J = 3.1 Hz, 1H), 6.67 (d, J = 15.9 Hz, 1H), 2.69 (s, 3H); ^{13}C NMR (126 MHz, CDCl$_3$, δ): 187.92, 150.35, 145.55, 143.65, 137.24, 135.38, 135.03, 133.83, 132.13, 131.69, 129.97, 129.85, 129.75, 129.42, 128.65, 127.35, 125.19, 123.30, 123.29, 122.95, 121.80, 121.44, 121.07, 120.70, 114.92, 110.64, 109.48, 105.11, 13.90; MS (M + H): for C$_{33}$H$_{24}$N$_6$O, calculated: 521.2089, observed: 521.2416.

3.3.15. (E)-1-(4-(1H-Indol-1-yl)phenyl)-3-(5-methoxy-3-methyl-1-phenyl-1H-pyrazol-4-yl)prop-2-en-1-one (14d).

Light tan solid; m.p. 182–184 °C; FT-IR (cm^{-1}): 3048.84, 1734.85, 1656.22, 1594.19, 1507.85, 1448.79, 1397.58, 1346.28, 1310.22, 1256.15, 1213.03, 1182.56, 1129.71, 1063.00, 1026.37, 966.18, 829.92, 753.19, 692.98, 652.80, 573.65, 519.25; ^{1}H NMR (500 MHz, CDCl$_3$, δ): δ 8.20 (d, J = 7.5 Hz, 2H), 7.86 (d, J = 15.5 Hz,

1H), 7.75–7.63 (m, 6H), 7.52–7.35 (m, 5H), 7.22 (d, J = 7.2 Hz, 1H), 6.75 (s, 1H), 3.89 (s, 3H), 2.50 (s, 3H); ^{13}C NMR (126 MHz, CDCl$_3$, δ): 188.91, 154.23, 149.36, 143.42, 137.79, 136.07, 135.48, 134.50, 130.06, 129.83, 129.31, 127.45, 127.42, 123.46, 122.91, 122.38, 121.43, 121.01, 118.62, 110.65, 104.99, 104.48, 61.92, 14.45; MS (M + H): for $C_{28}H_{23}N_3O_2$, calculated: 434.1868, observed: 434.2215.

3.3.16. (E)-1-(4-(1H-Pyrrol-1-yl)phenyl)-3-(3-methyl-1-phenyl-5-(piperidin-1-yl)-1H-pyrazol-4-yl)prop-2-en-1-one (15a).

Faint yellow solid; m.p. 160–164 °C; FT-IR (cm^{-1}): 3122.97, 2920.67, 2846.29, 1648.97, 1595.51, 1575.43, 1532.47, 1506.01, 1468.01, 1385.27, 1330.07, 1258.08, 1220.27, 1180.81, 1116.39, 1066.96, 1004.83, 976.59, 911.07, 858.51, 823.41, 757.59, 723.24, 686.40, 611.00; ^{1}H NMR (500 MHz, CDCl$_3$, δ): 8.10 (d, J = 8.6 Hz, 2H), 8.05 (d, J = 15.6 Hz, 1H), 7.53 (m, 4H), 7.46 (t, J = 7.8 Hz, 2H), 7.37 (t, J = 7.4 Hz, 1H), 7.26 (s, 1H), 7.21–7.15 (m, 2H), 6.46–6.34 (m, 2H), 3.08 (m, 4H), 2.51 (s, 3H), 1.57 (m, 6H); ^{13}C NMR (126 MHz, CDCl$_3$, δ): 188.82, 152.01, 148.89, 143.56, 139.66, 136.49, 135.70, 130.08, 129.01, 127.76, 124.82, 119.51, 119.07, 117.50, 111.48, 108.94, 52.23, 26.16, 23.84, 15.53; HRMS (ESI, M + H): for $C_{28}H_{28}N_4O$, calculated: 437.2341, observed: 437.2349; HRMS (M + H): for $C_{28}H_{28}N_4O$, calculated: 437.2341, observed: 437.2349.

3.3.17. (E)-1-(4-(1H-Pyrrol-1-yl)phenyl)-3-(3-methyl-5-morpholino-1-phenyl-1H-pyrazol-4-yl)prop-2-en-1-one (15b).

Yellow solid; m.p. 201–203 °C; FT-IR (cm^{-1}): 2960.86, 2840.10, 1658.94, 1596.39, 1495.72, 1433.08, 1381.14, 1334.42, 1271.28, 1218.05, 1183.30, 1114.15, 1067.59, 1014.13, 980.64, 917.18, 833.44, 756.38, 725.72, 689.84, 660.84, 609.73, 539.42; ^{1}H NMR (500 MHz, CDCl$_3$, δ): 8.10 (d, J = 8.0 Hz, 2H), 8.02 (d, J = 15.6 Hz, 1H), 7.48 (m, 7H), 7.30 (d, J = 15.7 Hz, 1H), 7.20 (s, 2H), 6.41 (s, 2H), 3.71 (s, 4H), 3.13 (s, 4H), 2.52 (s, 3H); ^{13}C NMR (126 MHz, CDCl$_3$, δ): 188.59, 150.17, 148.92, 143.69, 139.34, 135.64, 135.45, 130.11, 129.18, 128.22, 125.07, 119.52, 119.06, 118.42, 111.56, 109.40, 67.07, 50.98, 15.40; MS (M + H): for $C_{27}H_{26}N_4O_2$, calculated: 439.2134, observed: 439.2374.

3.3.18. (E)-3-(5-(1H-Benzo[d][1,2,3]triazol-1-yl)-3-methyl-1-phenyl-1H-pyrazol-4-yl)-1-(4-(1H-pyrrol-1-yl)phenyl)prop-2-en-1-one(15c).

Off white solid; m.p. 244–247 °C; FT-IR (cm^{-1}): 1658.12, 1601.63, 1498.17, 1436.53, 1387.77, 1336.34, 1291.99, 1223.41, 1183.19, 1119.01, 1072.80, 1039.89, 1017.42, 971.10, 916.20, 870.34, 831.91, 744.33, 683.65, 608.93, 562.06, 520.14; ^{1}H NMR (500 MHz, CDCl$_3$, δ): 8.19 (d, J = 8.2 Hz, 1H), 7.66 (d, J = 8.5 Hz, 2H), 7.55 (d, J = 15.9 Hz, 1H), 7.48 (m, 2H), 7.37 (d, J = 8.5 Hz, 2H), 7.26–7.18 (m, 6H), 7.14 (s, 2H), 6.64 (d, J = 15.9 Hz, 1H), 6.38 (s, 2H), 2.67 (s, 3H); ^{13}C NMR (126 MHz, CDCl$_3$, δ): 187.72, 150.33, 145.53, 143.87, 137.24, 134.42, 133.81, 132.05, 131.45, 130.07, 129.72, 129.40, 128.62, 125.17, 123.28, 121.78, 120.68, 119.37, 119.00, 114.93, 111.64, 109.47, 13.84; MS (M + H): for $C_{29}H_{22}N_6O$, calculated: 471.1933, observed: 471.2197.

3.3.19. (E)-1-(4-(1H-Pyrrol-1-yl)phenyl)-3-(5-methoxy-3-methyl-1-phenyl-1H-pyrazol-4-yl)prop-2-en-1-one (15d).

Light tan solid; m.p. 165–167 °C; FT-IR (cm^{-1}): 2920.94, 2854.04, 1750.18, 1645.08, 1592.68, 1550.91, 1503.74, 1467.09, 1399.21, 1333.90, 1280.64, 1213.52, 1176.72, 1111.92, 1055.82, 970.25, 912.29, 825.91, 772.85, 727.41, 687.77, 664.25, 608.52, 570.19, 519.07; ^{1}H NMR (500 MHz, CDCl$_3$, δ): 8.11 (d, J = 8.3 Hz, 2H),

7.82 (d, J = 15.6 Hz, 1H), 7.70 (m, 2H), 7.55–7.33 (m, 6H), 7.19 (s, 2H), 6.40 (s, 2H), 3.88 (s, 3H), 2.48 (s, 3H); ^{13}C NMR (126 MHz, CDCl$_3$, δ): 188.75, 154.18, 149.31, 143.70, 137.80, 135.42, 134.27, 130.17, 129.30, 127.39, 122.35, 119.51, 119.06, 118.65, 111.55, 104.45, 61.89, 14.43; MS (M + H): for $C_{24}H_{21}N_3O_2$, calculated: 384.1712, observed: 384.1630.

3.4. Acute oral toxicity

The acute oral toxicity study of the synthesized compounds was conducted on female Swiss albino mice following OECD 423 guidelines to determine the toxicity class based on mortality rates and clinical signs at defined dose levels. The results facilitated classification according to the Globally Harmonized System (GHS) for chemicals causing acute toxicity. Female Swiss albino mice (20–23 g) were housed under controlled conditions (22 ± 3 °C, 50–65% humidity, 12-hour light/dark cycle) with free access to feed and water. The study was approved by the Institutional Animal Ethics Committee (approval date: 28 January 2024; approval no.: Biotox/IAEC/03/2024/RP-23B). The OECD 423 guideline employs the Acute Oral Toxic Class method, a stepwise procedure using a minimal number of animals to assess acute toxicity. The test substance was administered orally at predefined doses, with each step involving three female mice. The test aimed to classify the compound into predefined toxicity classes based on LD$_{50}$ cut-off values. In step 1, three female mice were administered the synthesized compounds (diluted in distilled water) at 300 mg per kg body weight using a stainless steel intubation needle fitted to a graduated syringe. Feed was withheld 3–4 hours before and 2 hours after dosing, while water was available ad libitum. The animals were monitored for 14 days post-dosing for clinical signs and mortality. In step 2, another group of three female mice received the synthesized compounds at 2000 mg per kg body weight under identical conditions. The observation period was again 14 days post-dosing. The test compounds (13a–13c) were evaluated systematically, and the toxicity classification was determined based on the observed outcomes. Animals were monitored closely post-dosing, with observations at least once in the first 30 minutes, periodically during the first 24 hours (especially the initial 4 hours), and daily for 14 days. Body weights were recorded before dosing (pre-administration fasting weight) and on day 7 and day 15 (or at death). Since the fixed dose method does not determine a precise LD$_{50}$ value, no statistical analysis was performed. The classification of the synthesized compounds followed GHS guidelines based on LD$_{50}$ values.

3.5. Antidepressant activity by tail suspension method

Female Swiss albino mice, weighing between 20 and 23 grams, were utilized for this study. The animals were housed under controlled environmental conditions, with free access to standard laboratory feed and water. The experimental room was maintained at a temperature of 22 ± 3 °C, a relative humidity of 50–65%, and a 12-hour light/dark cycle to ensure optimal physiological conditions. The experimental protocol was reviewed and approved by the Institutional Animal Ethics Committee on 28th January 2024 (approval number: Biotox/IAEC/03/2024/RP-23B),

ensuring compliance with ethical standards for animal research. The Tail Suspension Test (TST), a well-established behavioral paradigm, was employed to assess "depression-like" behavior and learned helplessness in mice. This test is widely recognized for its utility in screening potential antidepressant compounds and evaluating interventions that may influence depression-related behaviors. During the TST, mice were individually suspended by their tails from a hook within a three-sided chamber, preventing escape or contact with nearby surfaces. The primary behavioral endpoint measured was the duration of immobility, which serves as an indicator of depressive-like behavior. Thirty minutes prior to the test, mice were administered either standard or test compounds. Each animal was suspended 50 cm above the surface, with its body oriented downward. Typically, mice attempt to escape the aversive situation by climbing or moving, but those exhibiting depressive-like behavior tend to cease struggling and remain immobile. The total duration of immobility during the 10-minute test period was recorded, with prolonged immobility reflecting a state of behavioral despair.

3.6. Antidepressant activity by forced swim test

Female Swiss albino mice, weighing 20–23 grams, were utilized in this study under controlled environmental conditions, including a temperature of 22 ± 3 °C, relative humidity of 50–65%, and a 12-hour light/dark cycle. The animals were provided with free access to standard feed and water, ensuring their well-being throughout the experiment. The study protocol was approved by the Institutional Animal Ethics Committee on 28th January 2024 (approval number: Biotox/IAEC/03/2024/RP-23B), adhering to ethical guidelines for animal research. The Forced Swim Test (FST), a widely recognized behavioral assay developed by Porsolt *et al.* in 1977, was employed to evaluate "depressive-like" states and behavioral despair in mice. This test is a gold standard for screening the efficacy of potential antidepressant compounds. Mice were administered standard or test drugs 30 minutes prior to the test. Swimming activity was defined as horizontal movement within the swim cylinder, while immobility was characterized by the absence of movement except for minimal efforts to keep the mouse's head above water. The FST consisted of two sessions conducted 24 hours apart. The first session, a 10-minute pre-test, was conducted one day prior to the main test to acclimate the animals to the experimental conditions. The main test, also lasting 10 minutes, was performed the following day. The swim cylinders were filled with tap water maintained at 23 ± 1 °C, with the water depth adjusted to prevent the mice from touching the bottom with their hind legs. After each session, mice were removed, dried, and returned to their housing. The water was replaced after each trial to eliminate potential confounding factors. The duration of swimming and immobility was meticulously recorded for each animal, providing quantitative measures of depressive-like behavior. To evaluate the antidepressant activity of the synthesized compounds, the mice were divided into multiple experimental groups. Group-I (Positive Control) received saline (10 mL kg^{-1}) with no additional treatment. Group-II (Standard) was administered fluoxetine, a well-

established antidepressant, at a dose of 10 mg kg^{-1}. Groups-III to XIV was treated with the synthesized compounds at a dose of 100 mg kg^{-1}. This experimental design enabled a comprehensive comparison between the positive control, standard antidepressant, and the test compounds, offering critical insights into their potential antidepressant efficacy. The systematic administration of treatments and doses ensured a robust and reliable evaluation of the compounds' effects on depressive-like behavior in the FST model.

3.7. Molecular docking

Molecular docking studies were carried out *via* GLIDE (Grid-Based Ligand Docking with Energetics) programme of the Schrödinger molecular modeling software (Schrödinger, LLC, New York, NY).[65–67] To gauge the binding affinity of the synthesised chalcones towards the active site of human serotonin transporter receptor. The crystal structure of the receptor complexed with Paroxetine (PDB code: 5I6X) was obtained from the RCSB Protein Data Bank and then refined for docking through the Protein Preparation Wizard using the OPLS-2005 force field. This involved elimination of the crystallographic water molecules since no conserved interactions with receptor; appending the missing protons/side chain atoms corresponding to pH 7.0 and assignment of appropriate charge and protonation state. The refined structure thus obtained was energy minimized to relieve the steric clashes among the amino acid residues till RMSD for the heavy atoms reached 0.30 Å. The 3D structures of the chalcone derivatives were sketched using the build panel in Maestro and optimized using Ligand Preparation tool which included adjusting realistic bond lengths and angles, assignment of the partial charges using the OPLS-2005 force-field and final energy minimization until the RMSD of heavy atoms reached 0.001 Å. Next, the shape and properties of the active site were defined through using the Receptor Grid Generation panel for which a grid box of $10 \times 10 \times 10$ Å dimensions centered on the centroid of the co-crystallized ligand was generated. With this setup, the chalcone derivatives were subjected to molecular docking for determining the binding affinities and modes of interactions of the towards human serotonin transporter receptor using the extra precision (XP) Glide scoring function. The docking conformations were visualized and analyzed for the most significant elements of thermodynamic interactions using the Maestro's Pose Viewer utility.

3.8. ADME

To assess the pharmacokinetic and drug-like properties of the synthesized compounds, their ADME profiles were determined using the SwissADME online platform (http://www.swissadme.ch/).[63] Chemical structures were converted from ChemDraw to SMILES strings, which were then analyzed by the tool. SwissADME generated data on key physicochemical properties, hydrogen bonding capacity, lipophilicity, TPSA, and water solubility, alongside pharmacokinetic parameters such as GI absorption, BBB permeability, P-gp substrate status, and CYP inhibition. Drug-

likeness was evaluated using Lipinski's Rule of Five, Veber's Rule, Ghose filter, Egan's Rule, and Muegge's Rule.

3.9. DFT method

DFT method is widely used to analyze the electronic properties, stability, and reactivity of many small organic molecules offering insights for applications in chemistry and pharmacology.[68–70] All DFT computations for the synthesized compound (**13c**) were carried out in the gas phase using the Gaussian 03 software.[71] The calculations employed Becke's three-parameter hybrid exchange functional (B3LYP).[72,73] with the 6-31G(d,p) basis set. Molecular visualization was performed using the GaussView 4.1.2 program.[74]

4 Conclusion

Twelve novel nitrogen-containing heterocycle-linked chalcone derivatives were synthesized and evaluated for antidepressant activity. *In vivo* assessment using the Tail Suspension Test and Forced Swim Test revealed that compounds bearing the benzo[*d*][1,2,3]triazol-1-yl moiety significantly reduced immobility duration, highlighting their potent antidepressant potential, whereas derivatives containing piperidin-1-yl and morpholino groups exhibited comparatively modest activity. These compounds demonstrated strong binding affinity to the human serotonin transporter (hSERT) through molecular docking, supported by favorable pharmacokinetic properties and low acute oral toxicity ($LD_{50} > 2000$ mg kg^{-1}). Molecular docking against Human Serotonin Transporter (hSERT) could provide insights into the mechanistic basis of antidepression activity. The *in silico* binding affinity data for the all chalcones were found to be in agreement with the observed antidepression activity. The per-residue interaction analysis could identify the significant thermodynamic interactions with active site residues which are being utilized to carry out site specific modifications of the chalcone scaffold to arrive at compounds with higher affinity and selectivity towards hSERT. These findings underscore the compounds' potential as safe and effective antidepressant agents, warranting further development and optimization for therapeutic applications.

Ethical approval

The Institutional Animal Ethics Committee approved the experimental protocol (approval date: 28/January/2024; void number: Biotox/IAEC/03/2024/RP-23B).

Data availability

The data supporting this article have been included as part of the ESI.†

Author contributions

H. S. D., V. A. A., and B. S. J. conceived and designed the study. H. S. D. synthesized the compounds. H. S. D., V. A. A., and S. B. W. conducted spectral analysis. V. M. K. performed molecular docking and ADME studies. H. S. D., V. A. A. and V. M. K. wrote the manuscript with input from all authors. All authors reviewed and approved the final manuscript.

Conflicts of interest

There are no conflicts to declare.

Acknowledgements

References

1 H. Jia, M. M. Zack, W. W. Thompson, A. E. Crosby and I. I. Gottesman, *Soc. Psychiatr. Psychiatr. Epidemiol.*, 2015, **50**, 939.

2 A. Pannu and R. K. Goyal, *Curr. Drug Saf.*, 2025, **20**(2), 120–147.

3 S. B. Tsogoeva, *Mini-Rev. Med. Chem.*, 2010, **10**, 773.

4 K. Singh, R. Pal, S. A. Khan, B. Kumar and M. J. Akhtar, *J. Mol. Struct.*, 2021, **1237**, 130369.

5 B. C. Revanasiddappa, M. V. Kumar and H. Kumar, *Dhaka Univ. J. Pharm. Sci.*, 2020, **19**, 179.

6 N. A. Elkanzi, H. Hrichi, R. A. Alolayan, W. Derafa, F. M. Zahou and R. B. Bakr, *ACS Omega*, 2022, 7, 27769.

7 M. J. Matos, S. Vazquez-Rodriguez, E. Uriarte and L. Santana, *Expert Opin. Ther. Pat.*, 2015, **25**, 351.

8 J. Dong, G. Huang, Q. Zhang, Z. Wang, J. Cui, Y. Wu, Q. Meng and S. Li, *MedChemComm*, 2019, **10**, 1606.

9 J. Dong, Q. Zhang, Q. Cui, G. Huang, X. Pan and S. Li, *ChemMedChem*, 2016, **11**, 2102.

10 M. Rudrapal, J. Khan, A. A. B. Dukhyil, R. M. I. I. Alarousy, E. I. Attah, T. Sharma, S. J. Khairnar and A. R. Bendale, *Molecules*, 2021, **26**, 7177.

11 A. Yadav, V. Sharma and G. Singh, *ChemistrySelect*, 2024, **9**, e202401321.

12 S. S. Sankhe and V. M. Mukadam, *Results Chem.*, 2024, **9**, 101633.

13 A. Maurya and A. Agrawal, *Mini-Rev. Med. Chem.*, 2024, **24**, 176.

14 S. Patel and S. Mishra, *Curr. Org. Chem.*, 2024, **28**, 32.

15 B. Ardiansah, *J. Appl. Pharm. Sci.*, 2019, **9**, 117.

16 K. Mezgebe, Y. Melaku and E. Mulugeta, *ACS Omega*, 2023, **8**, 19194.

17 M. M. Heravi and V. Zadsirjan, *RSC Adv.*, 2020, **10**, 44247.

18 D. K. Lang, R. Kaur, R. Arora, B. Saini and S. Arora, *Anti-Cancer Agents Med. Chem.*, 2020, **20**, 2150.

19 Y. N. Nayak, S. L. Gaonkar and M. Sabu, *J. Heterocycl. Chem.*, 2023, **60**, 1301.

20 M. T. Albuquerque, M. M. Santos, C. A. S. Cavaleiro and A. M. S. Silva, *Curr. Org. Chem.*, 2014, **18**, 2750.

21 Z. W. Mao, X. Zheng, Y. P. Lin, Y. Qi, C. Hu, C. Wan and G. Rao, *Heterocycles*, 2016, **92**, 1102.

22 Y. Kim, M. Yeom, J. Tae, H. Rhim and H. Choo, *Eur. J. Med. Chem.*, 2016, **110**, 302.

23 R. R. Kumar, V. Kumar, D. Kaur, N. K. Nandi, A. R. Dwivedi, V. Kumar and B. Kumar, *ChemistrySelect*, 2021, **6**, 11276.

24 M. Z. Wróbel, A. Chodkowski, F. Herold, M. Marciniak, M. Dawidowski, A. Siwek, G. Starowicz, K. Stachowicz, B. Szewczyk, G. Nowak and M. Belka, *Eur. J. Med. Chem.*, 2019, **183**, 111736.

25 S. S. Fatahala, S. Nofal, E. Mahmoud and R. H. Abd El-hameed, *Med. Chem.*, 2019, **15**, 911.

26 O. Afzal, S. Bawa, S. Kumar, R. Kumar and M. Q. Hassan, *Lett. Drug Des. Discovery*, 2013, **10**, 75.

27 A. P. Kourounakis, D. Xanthopoulos and A. Tzara, *Med. Res. Rev.*, 2020, **40**, 709.

28 A. Rani, A. Singh, J. Kaur, G. Singh, R. Bhatti, N. Gumede, P. Kisten, P. Singh and V. Kumar, *Bioorg. Chem.*, 2021, **114**, 105053.

29 J. Higgs, C. Wasowski, A. Marcos, M. Jukič, C. H. Paván, S. Gobec, F. de Tezanos Pinto, N. Colettis and M. Marder, *Heliyon*, 2019, **5**, e01324.

30 B. Mathew, D. G. Parambi, V. S. Sivasankarapillai, M. S. Uddin, J. Suresh, G. E. Mathew, M. Joy, A. Marathakam and S. V. Gupta, *CNS Neurol. Disord.:Drug Targets*, 2019, **18**, 432.

31 K. Singh, R. Pal, S. A. Khan, B. Kumar and M. J. Akhtar, *J. Mol. Struct.*, 2021, **1237**, 130369.

32 A. A. Asselin, L. G. Humber, J. Komlossy and M. P. Charest, *J. Med. Chem.*, 1976, **19**, 792.

33 M. E. Freed, E. Hertz and L. M. Rice, *J. Med. Chem.*, 1964, **7**, 628.

34 G. F. Makhaeva, N. P. Boltneva, N. V. Kovaleva, E. V. Rudakova, S. V. Lushchekina, A. Y. Aksinenko and V. B. Sokolov, *Russ. Chem. Bull.*, 2018, **67**, 1724.

35 P. O. Patil and S. B. Bari, *Arabian J. Chem.*, 2016, **9**, 588.

36 P. O. Patil and S. B. Bari, *J. Chem.*, 2013, **2013**, 637205.

37 R. A. Rane, S. Napahde, P. K. Bangalore, N. U. Sahu, N. Shah, Y. A. Kulkarni, K. Barve, L. Lokare and R. Karpoormath, *Chem. Biol. Drug Des.*, 2014, **84**, 593.

38 A. Boido, C. C. Boido and F. Sparatore, *Il Farmaco*, 2001, **56**, 263.

39 S. Tsutsumi, L. Gündisch and D. Sun, *Curr. Top. Med. Chem.*, 2016, **16**, 1290.

40 M. Bashir, A. Bano, A. S. Ijaz and B. A. Chaudhary, *Molecules*, 2015, **20**, 13496.

41 P. V. Thanikachalam, R. K. Maurya, V. Garg and V. Monga, *Eur. J. Med. Chem.*, 2019, **180**, 562.

42 S. Y. Kang, E. J. Park, W. K. Park, H. J. Kim, D. Jeong, M. E. Jung, K. S. Song, S. H. Lee, H. J. Seo, M. J. Kim and M. Lee, *Bioorg. Med. Chem. Lett.*, 2010, **20**, 1705.

43 K. Singh, R. Pal, S. A. Khan, B. Kumar and M. J. Akhtar, *J. Mol. Struct.*, 2021, **1237**, 130369.

44 A. Kumari and R. K. Singh, *Bioorg. Chem.*, 2020, **96**, 103578.

45 G. Caliendo, G. Greco, P. Grieco, E. Novellino, E. Perissutti, V. Santagada, D. Barbarulo, E. Esposito and A. De Blasi, *Eur. J. Med. Chem.*, 1996, **31**, 207.

46 J. P. C. Chang, A. Zamparelli, M. Nettis and C. Pariante, *Encyclopedia of Behavioral Neuroscience*, ed. S. D. Sala, 2nd edn, 2022, pp. 613.

47 J. L. B. Saayman, B. H. Harvey, G. Wegener and C. B. Brink, *Eur. J. Pharmacol.*, 2024, **969**, 176434.

48 E. H. Hassanein, H. S. Althagafy, M. A. Baraka, E. K. Abd-Alhameed and I. M. Ibrahim, *Naunyn-Schmiedeberg's Arch. Pharmacol.*, 2024, **397**, 2603.

49 A. Fagiolini, A. González-Pinto, K. W. Miskowiak, P. Morgado, A. H. Young and E. Vieta, *Ann. Gen. Psychiatr.*, 2023, **22**, 32.

50 S. Schiavone, P. Tucci, E. Mhillaj, M. Bove, L. Trabace, M. G. Morgese and P. Neuro-Psychopharmacol, *Biol. Psychiatry*, 2017, **78**, 114.

51 M. Kowalska, J. Nowaczyk, Ł. Fijałkowski and A. Nowaczyk, *Int. J. Mol. Sci.*, 2021, **22**, 1662.

52 A. J. Cross, D. Widzowski, C. Maciag, A. Zacco, T. Hudzik, J. Liu, S. Nyberg and M. W. Wood, *Br. J. Pharmacol.*, 2016, **173**, 155.

53 Y. Kim, M. Yeom, J. Tae, H. Rhim and H. Choo, *Eur. J. Med. Chem.*, 2016, **110**, 302.

54 R. R. Kumar, V. Kumar, D. Kaur, N. K. Nandi, A. R. Dwivedi, V. Kumar and B. Kumar, *ChemistrySelect*, 2021, **6**, 11276–11284.

55 S. Shi, D. Ma, X. Guo, Y. Chen, J. Yu, X. Hu, X. Wang, T. Li, K. Wang, Y. Zhi and G. Yang, *J. Med. Chem.*, 2024, **67**, 10350.

56 S. Y. Kang, E. J. Park, W. K. Park, H. J. Kim, G. Choi, M. E. Jung, H. J. Seo, M. J. Kim, A. N. Pae, J. Kim and J. Lee, *Bioorg. Med. Chem.*, 2010, **18**, 6156.

57 D. Choudhary, B. Kumar, B. Chandrasekaran, T. G. Singh, R. Kaur, A. Aldahish, R. Vasudevan and P. Balaji, *Pharmaceuticals*, 2025, **18**, 309.

58 G. Caliendo, R. Di Carlo, R. Meli, E. Perissutti, V. Santagada, C. Silipo and A. Vittoria, *Eur. J. Med. Chem.*, 1993, **28**, 969.

59 F. Artigas, *ACS Chem. Neurosci.*, 2013, **4**, 5.

60 G. Ślifirski, M. Król and J. Turło, *Int. J. Mol. Sci.*, 2021, **22**, 9015.

61 R. H. Waghchaure and V. A. Adole, *J. Mol. Struct.*, 2024, **1296**, 136724.

62 V. A. Adole, *Organomet. Chem.*, 2021, **1**, 29.

63 A. Daina, O. Michielin and V. Zoete, *Sci. Rep.*, 2017, **7**, 42717.

64 K. B. Gangurde, R. A. More, V. A. Adole and D. S. Ghotekar, *J. Mol. Struct.*, 2024, **1299**, 136760.

65 R. A. Friesner, R. B. Murphy, M. P. Repasky, L. L. Frye, J. R. Greenwood, T. A. Halgren, P. C. Sanschagrin and D. T. Mainz, *J. Med. Chem.*, 2006, **49**, 6177–6196.

66 T. A. Halgren, R. B. Murphy, R. A. Friesner, H. S. Beard, L. L. Frye, W. T. Pollard and J. L. Banks, *J. Med. Chem.*, 2004, **47**, 1750.

67 R. A. Friesner, J. L. Banks, R. B. Murphy, T. A. Halgren, J. J. Klicic, D. T. Mainz, M. P. Repasky, E. H. Knoll, M. Shelley, J. K. Perry and D. E. Shaw, *J. Med. Chem.*, 2004, **47**, 1739.

68 V. A. Adole, A. Kumar, N. Misra, R. A. Shinde and B. S. Jagdale, *Polycyclic Aromat. Compd.*, 2024, **44**(8), 5397–5411.

69 K. B. Gangurde, V. A. Adole and D. S. Ghotekar, *Results Chem.*, 2023, **6**, 101093.

70 V. A. Adole, *Organomet. Chem.*, 2021, **1**, 29.

71 M. J. Frisch, G. W. Trucks, H. B. Schlegel, G. E. Scuseria, M. A. Robb, J. R. Cheeseman, V. G. Zakrzewski, J. A. Montgomery Jr, T. Vreven, K. N. Kudin and J. C. Burant, *Gaussian 03, Revision C.02*, Gaussian, Inc., Wallingford CT, 2004.

72 A. D. Becke, *J. Chem. Phys.*, 1993, **98**, 5648.

73 C. Lee, W. Yang and R. G. Parr, *Phys. Rev. B:Condens. Matter Mater. Phys.*, 1988, **37**, 785.

74 R. D. Dennington II, T. Keith and J. Millam, *GaussView, Version 4.1.2*, Semichem Inc., Shawnee Mission, KS, 2007.